bioRxiv preprint doi: https://doi.org/10.1101/2021.09.12.459970; this version posted September 12, 2021. The copyright holder for this preprint (which was not certified by peer review) is the author/funder, who has granted bioRxiv a license to display the preprint in perpetuity. It is made available under aCC-BY-NC 4.0 International license.

Activation of the CaMKII-Sarm1-ASK1 MAP kinase pathway protects against axon degeneration caused by loss of mitochondria

Chen Ding[1], Youjun Wu[2], Hadas Dabas[2], and Marc Hammarlund[1,2,*]

[1]Department of Neuroscience, Yale University School of Medicine, New Haven, CT, 06510, USA

[2]Department of Genetics, Yale University School of Medicine, New Haven, CT, 06510, USA

[*]Correspondence: marc.hammarlund@yale.edu

Abstract

Mitochondrial defects are tightly linked to axon degeneration, yet the underlying cellular mechanisms remain poorly understood. In *C. elegans,* PVQ axons that lack mitochondria degenerate spontaneously with age. Using an unbiased genetic screen, we found that cell-specific activation of CaMKII/UNC-43 suppresses axon degeneration due to loss of mitochondria. Unexpectedly, CaMKII/UNC-43 protects against degeneration through the conserved Sarm1/TIR-1-ASK1/NSY-1 MAPK pathway. In addition, we show that disrupting a trafficking complex composed of calsyntenin/CASY-1, Mint/LIN-10, and kinesin suppresses axon degeneration. Further analysis indicates that disruption of this trafficking complex activates the CaMKII-Sarm1-MAPK pathway through L-type voltage-gated calcium channels. Our findings identify CaMKII as a pivot point between mitochondrial defects and axon degeneration, describe how it is regulated in this context, and uncover a surprising neuroprotective role for the Sarm1-ASK1 pathway.

bioRxiv preprint doi: https://doi.org/10.1101/2021.09.12.459970; this version posted September 12, 2021. The copyright holder for this preprint (which was not certified by peer review) is the author/funder, who has granted bioRxiv a license to display the preprint in perpetuity. It is made available under aCC-BY-NC 4.0 International license.

Introduction

Mitochondria are abundant in axons and at most synapses. The critical importance of these distal mitochondria is highlighted by the close relationship between defects in mitochondria localization or function and multiple neurodegenerative diseases. For some forms of hereditary neurodegeneration, such as hereditary spastic paraplegias, dominant optic atrophy, and Charcot-Marie-Tooth hereditary neuropathy type 2A (CMT2A), mutations in genes encoding distinct mitochondrial proteins are thought to be causative (Alavi and Fuhrmann, 2013; Blackstone, 2018; Zuchner et al., 2004). Additionally, familial forms of Parkinson's disease arise from defective mitochondria quality control associated with mutations in the PINK1 and Parkin genes (Pickrell and Youle, 2015). Mitochondrial dysfunction has also been suggested to play roles in the more common, sporadic, forms of both Parkinson's Disease and Alzheimer's disease (Grunewald et al., 2019; Hauptmann et al., 2006). However, the cellular mechanisms that determine the neurodegenerative response to mitochondria mislocalization or dysfunction are not well understood.

One well-established prodegenerative pathway in neurons involves dysregulated calcium homeostasis. For example, in neurodegenerative diseases including Alzheimer's disease (AD), Parkinson's disease (PD), Huntington's disease (HD), and amyotrophic lateral sclerosis (ALS), elevated intracellular calcium levels have been observed. Proposed mechanisms resulting in elevated calcium include weakening of calcium buffering capacity, deregulation of calcium channel activities, and disruption of mitochondrial calcium homeostasis (Bezprozvanny, 2009; Marambaud et al., 2009; Zundorf and Reiser, 2011). Excess cytosolic calcium activates the calpain family of Ca^{2+}-dependent proteases, which cleave a variety of neuronal substrates and lead to degeneration (Camins et al., 2006). Ca^{2+}/calmodulin-dependent protein kinase II (CaMKII) has also been shown to mediate neurodegeneration in the context of elevated intracellular calcium levels (Hou et al., 2009; Woolums et al., 2020). In addition, elevated calcium causes mitochondrial malfunctions (Bezprozvanny, 2009). Mitochondria can buffer cytosolic calcium through the mitochondrial Ca^{2+} uniporter (MCU), and can release their calcium content through the mitochondrial permeability transition pore (mPTP) (Halestrap, 2009; Hoppe, 2010). Mitochondria calcium overload, together with mitochondrial depolarization and oxidative stress, can trigger the opening of mPTP, which also leads to the release of apoptotic factors and triggers cell death (Halestrap, 2009). Thus, elevated calcium can promote neurodegeneration via various mechanisms.

bioRxiv preprint doi: https://doi.org/10.1101/2021.09.12.459970; this version posted September 12, 2021. The copyright holder for this preprint (which was not certified by peer review) is the author/funder, who has granted bioRxiv a license to display the preprint in perpetuity. It is made available under aCC-BY-NC 4.0 International license.

More recently, a second major prodegenerative pathway in neurons was identified, centered on Sarm1. Sarm1 is essential for Wallerian degeneration in flies and mammals (Gerdts et al., 2013; Osterloh et al., 2012) and has a role in selected additional degeneration models such as traumatic brain injury (Henninger et al., 2016) and peripheral neuropathy (Turkiew et al., 2017). The Sarm1 TIR domains possess intrinsic NAD^+ hydrolase activity (Essuman et al., 2017), and activation of Sarm1 rapidly depletes NAD^+ in axons, leading to metabolic catastrophe and eventually axon degeneration (Gerdts et al., 2015). In addition to NAD^+ metabolism, Sarm1 has been shown to activate MAPK pathways (Chuang and Bargmann, 2005; Hsu et al., 2020; Yang et al., 2015). The role of MAPK signaling was examined in Wallerian degeneration, but mixed results were reported. Two studies showed that the c-Jun N-terminal kinase (JNK) MAPK pathway promotes axon degeneration, although its epistatic relationship with Sarm1 remains controversial (Walker et al., 2017; Yang et al., 2015). However, an *in vivo* study in *Drosophila* argues against the requirement of JNK signaling in axon degeneration (Neukomm et al., 2017). Sarm1 also contains a mitochondrial targeting sequence (MTS) for association with the outer mitochondrial membrane (Panneerselvam et al., 2012). However, the importance of interactions between Sarm1 and mitochondria is still unclear, as cytosolic Sarm1 protein lacking MTS is fully capable of activating degeneration and mitochondrial shape and motility is unaffected in Sarm1 KO neurons (Gerdts et al., 2013; Summers et al., 2014).

In this study, to identify cellular mechanisms that oppose or promote neurodegeneration in response to mitochondria dysfunction, we analyzed a *C. elegans* model of axon degeneration caused by complete absence of axonal mitochondria (Rawson et al., 2014). Using an unbiased approach, we discovered that Ca^{2+}/calmodulin-dependent protein kinase II (CaMKII/UNC-43) activity cell-autonomously protects against degeneration, even though mitochondria mislocalization persists. We found that CaMKII/UNC-43 abundance in axons is greatly reduced in the absence of mitochondria, suggesting that CaMKII/UNC-43 insufficiency is a key pivot point that links the loss of mitochondria to axon degeneration. Surprisingly, axon protection by CaMKII/UNC-43 requires Sarm1/TIR-1 and the downstream NSY-1-SEK-1 mitogen-activated protein kinase (MAPK) pathway (Chuang and Bargmann, 2005; Hayakawa et al., 2006). Finally, we found that loss of the conserved axonal transport factors calsyntenin or Mint suppresses axon degeneration, and that this suppression is dependent on L-type voltage-gated calcium channel and

bioRxiv preprint doi: https://doi.org/10.1101/2021.09.12.459970; this version posted September 12, 2021. The copyright holder for this preprint (which was not certified by peer review) is the author/funder, who has granted bioRxiv a license to display the preprint in perpetuity. It is made available under aCC-BY-NC 4.0 International license.

CaMKII/UNC-43. Together, our data provide insight into the cellular mechanisms that control the neurodegenerative response to mitochondria mislocalization, and reveal a novel anti-degenerative function for Sarm1, calcium, and CaMKII.

Results

An unbiased screen identifies suppressors of axon degeneration caused by lack of mitochondria

In *C. elegans*, anterograde traffic of mitochondria from neuronal cell bodies to axons is known to depend on a small number of factors: *unc-116*, which encodes the kinesin heavy chain (KHC) of the kinesin-1 motor complex (Schwarz, 2013); the novel factor *ric-7*, which is specifically required for mitochondria localization in axons (Rawson et al., 2014); and the combined activity of Miro, Milton and metaxin, which couple mitochondria to kinesin-1-mediated traffic (Glater et al., 2006; Guo et al., 2005; Stowers et al., 2002; Zhao et al., 2021). The two PVQ neurons are a pair of unipolar neurons in the posterior of the animal that each extends a single long neurite to the nerve ring in the head (Figure 1A). PVQ was previously shown to degenerate as a result of lack of axonal mitochondria in *ric-7* mutants (Rawson et al., 2014). We labeled both PVQ neurons with the *oyIs14[sra-6p::GFP]* transgene (which additionally marks the ASI and ASH neurons in the head) (Nolan et al., 2002) (Figure 1C). We also labeled mitochondria in PVQ using a TagRFP marker targeted to the mitochondria matrix (mito::TagRFP) with the mitochondrial import signal from chicken aspartate aminotransferase (Figure 1E) (Ghose et al., 2013; Jaussi et al., 1985). We quantified degeneration by determining the fraction of animals with no PVQ degeneration (two intact non-truncated PVQ axons) (Figure 1B). Consistent with previous findings (Rawson et al., 2014), loss of *ric-7* results in a complete absence of mitochondria in PVQ axons as early as the L1 stage, which continues into and past the L4 stage (Figure 1E-1G). The loss of axonal mitochondria is accompanied by completely penetrant degeneration of PVQ axons in adults (Figure 1C-1D). Most axons degenerate during the L4 to 1-day-old adult (1doa) transition (Figure 1D). Similarly, PVQ axons also degenerate in KHC/*unc-116* mutants and Miro-metaxin/*miro-1; mtx-2* double mutants (Figure 1-figure supplement 1A), in which mitochondria are completely absent in axons (Rawson et al., 2014; Zhao et al., 2021). By contrast, PVQ axons do not degenerate in *miro-1; miro-2* double mutants or in Milton/*trak-1* single mutants (Figure 1-figure supplement 1A), likely because mitochondria are still present

bioRxiv preprint doi: https://doi.org/10.1101/2021.09.12.459970; this version posted September 12, 2021. The copyright holder for this preprint (which was not certified by peer review) is the author/funder, who has granted bioRxiv a license to display the preprint in perpetuity. It is made available under aCC-BY-NC 4.0 International license.

in axons in these mutants (Sure et al., 2018; Zhao et al., 2021). Therefore, spontaneous PVQ axon degeneration is induced by the complete loss of axonal mitochondria. Because kinesin-1 is involved in the transport of multiple axonal cargoes in addition to mitochondria (Guedes-Dias and Holzbaur, 2019), we used *ric-7* mutants for further analysis of the relationship between axonal mitochondria and degeneration.

End-stage PVQ degeneration is visible in *ric-7* mutants as truncated axons that are disconnected from the nerve ring (Figure 1A-1C). To determine the sequence of events that leads to degeneration, we performed longitudinal imaging of individual axons. We found that degeneration is a sequential process beginning with axon swelling, progressing through thinning and fragmentation, and ending with debris clearance (Figure 1H). To further confirm that PVQ axon degeneration in *ric-7* mutants is caused by the absence of mitochondria, we expressed a chimeric construct consisting of the UNC-116/Kinesin-1 motor and the mitochondrial outer membrane protein TOMM-7, which restores axonal mitochondria localization, and we found that degeneration could be completely suppressed (Figure 1-figure supplement 1B-1C) (Nichols et al., 2016; Rawson et al., 2014). Thus, the PVQ axon in *ric-7* mutants is a completely penetrant system for analyzing axon degeneration caused by loss of axonal mitochondria.

To identify molecular mechanisms required for axon degeneration in the absence of mitochondria, we performed an unbiased suppressor screen in the *ric-7(n2657)* background (Figure 1A). After standard EMS mutagenesis and screening of semi-clonal F2s (see Methods), we recovered 11 strains with >50% suppression of degeneration (Figure 1B). We cloned the two strongest suppressors, *wp64* and *wp60*, using whole genome sequencing (see Methods). *wp64* is an allele of *unc-43*, the *C. elegans* homolog of CaMKII, and *wp60* is an allele of *casy-1*, the *C. elegans* homolog of calsyntenin (Figure 1B and Figure 1-figure supplement 1D). In *ric-7(n2657); unc-43(wp64)* and *ric-7(n2657); casy-1(wp60)* animals, over 80% of 5doa have no degeneration—both PVQ axons are intact (Figure 1C-1D). However, despite the strong suppression of degeneration, mitochondria are still absent from axons in both suppressed strains at both the L1 and L4 stages (Figure 1E, 1F and 1G). Therefore, instead of restoring mitochondria localization in axons, the CaMKII/*unc-43(wp64)* and calsyntenin/*casy-1(wp60)* mutations maintain axon integrity in the absence of mitochondria.

bioRxiv preprint doi: https://doi.org/10.1101/2021.09.12.459970; this version posted September 12, 2021. The copyright holder for this preprint (which was not certified by peer review) is the author/funder, who has granted bioRxiv a license to display the preprint in perpetuity. It is made available under aCC-BY-NC 4.0 International license.

Constitutively-active CaMKII/UNC-43 suppresses spontaneous axon degeneration cell autonomously

The CaMKII/*unc-43(wp64)* allele is a G-to-A point mutation, which leads to a glycine to arginine substitution (G207R) in one of the two hydrophobic pockets of the catalytic domain (Figure 1-figure supplement 1D) (Umemura et al., 2005). This hydrophobic pocket interacts with T284 on the autoinhibitory domain and is critical for the autoinhibition of CaMKII in low calcium (Yang and Schulman, 1999). Abolishing this interaction with a T284D mutation in the autoinhibitory domain, or with a V206E mutation in the hydrophobic pocket, causes CaMKII/UNC-43 to be constitutively active even in the absence of calcium (Umemura et al., 2005; Yang and Schulman, 1999). Since the G207R alteration in our *wp64* allele is next to the V206E change that results in constitutive activity, we hypothesized that the *wp64* mutation also makes CaMKII/UNC-43 constitutively active. Indeed, the *unc-43(wp64)* worms display a dominant lethargic phenotype, similar to the canonical constitutively active *unc-43(n498sd)* mutants (Reiner et al., 1999). Further, we found that the *unc-43(n498sd)* mutation phenocopies *unc-43(wp64)* in terms of the anti-degeneration effect in *ric-7(n2657)* animals (Figure 2A). By contrast, the loss-of-function(lof) allele *unc-43(e408)* does not suppress degeneration in *ric-7(n2657)* animals (Figure 2A). Interestingly, although PVQ axons rarely degenerate when CaMKII/UNC-43 is activated, aberrant axonal swellings are still observed (Figure 2B), suggesting that degeneration is blocked at a step between initiation and severing. Mitochondria anterograde transport also requires Kinesin-1/UNC-116 (Hollenbeck and Saxton, 2005), and PVQ axons spontaneously degenerate in *unc-116(rh24sb79)* animals between L3 and L4 (Figure 2C). We found that constitutively active *unc-43(n498sd)* also suppresses degeneration in *unc-116(rh24sb79)* (Figure 2C). In conclusion, activated CaMKII/UNC-43 suppresses axon degeneration caused by the absence of mitochondria.

To examine if CaMKII/UNC-43 functions in PVQ cell autonomously, we overexpressed CaMKII/UNC-43 in PVQ in *ric-7(n2657)* animals. Expressing wildtype CaMKII/UNC-43 leads to mild but distinct protection against degeneration (20% of 3doa have no degeneration), while expressing a constitutively active (CA) form of CaMKII/UNC-43 (T284D) results in much stronger protection (70% of 3doa have no degeneration) (Figure 2A). These data indicate that active CaMKII/UNC-43 functions cell autonomously to suppress axon degeneration. Further, since overexpression of wildtype CaMKII/UNC-43

bioRxiv preprint doi: https://doi.org/10.1101/2021.09.12.459970; this version posted September 12, 2021. The copyright holder for this preprint (which was not certified by peer review) is the author/funder, who has granted bioRxiv a license to display the preprint in perpetuity. It is made available under aCC-BY-NC 4.0 International license.

158 has less effect on degeneration than expression of the constitutively active protein, our results suggest
159 that WT UNC-43 cannot be adequately activated even when overexpressed in PVQ axons without
160 mitochondria.

161 To explore potential mechanisms that might affect CaMKII/UNC-43 function in animals lacking
162 axonal mitochondria, we examined the abundance and distribution of CaMKII/UNC-43 protein using the
163 Native and Tissue-Specific Fluorescence (NATF) approach (He et al., 2019). Briefly, seven copies of the
164 GFP11 β-strand were knocked into the C terminus of the endogenous CaMKII/*unc-43* locus by
165 CRISPR/Cas9. The complementary split-GFP fragment GFP1-10 was then expressed under the PVQ
166 promoter, resulting in PVQ-specific labeling of CaMKII/UNC-43 at endogenous expression levels (Figure
167 2D). The *unc-43::gfp11x7* knock-in (KI) animals displayed no apparent uncoordinated or lethargic
168 phenotype related to *unc-43* mutants (data not shown), indicating that CaMKII/UNC-43 function is not
169 impaired by the KI. As a negative control, expressing GFP1-10 alone in PVQ did not produce visible GFP
170 fluorescence (Figure 2-figure supplement 1A). We examined the distribution of labeled CaMKII/UNC-43 in
171 control and *ric-7* animals at the L3 stage, which precedes spontaneous degeneration (Figure 1D)
172 (Rawson et al., 2014). We found that in *ric-7(n2657)* animals, CaMKII/UNC-43 abundance in distal axons
173 (posterior to the nerve ring) is dramatically reduced (37% of the control levels), while CaMKII/UNC-43
174 abundance in cell bodies is not affected (Figure 2D and 2E). Further, axonal CaMKII/UNC-43 abundance
175 in *ric-7(n2657)* animals was partially restored (to 69% of control levels) by expression of the UNC-
176 116::TOMM-7 chimeric protein, a synthetic method of forcing mitochondria into the axon in the absence of
177 *ric-7* (Rawson et al., 2014) (Figure 2D, 2E and Figure 1-figure supplement 1B). Therefore, our data
178 indicate that axonal mitochondria regulate CaMKII/UNC-43 localization in axons.

179 Does depletion of CaMKII from distal axons contribute to axon degeneration? To test this
180 possibility, we took advantage of our endogenously-tagged CaMKII/*unc-43* allele, in which the native
181 protein is fused with multiple tandem repeats of the GFP11 fragment (Figure 2F). In these animals we
182 expressed a fusion protein consisting of the GFP1-10 fragment and kinesin-1/UNC-116. We hypothesized
183 that *in vivo* reconstitution of GFP would link CaMKII/UNC-43 to kinesin, driving it into distal axons by
184 anterograde transport, while at the same time enabling visualization of CaMKII/UNC-43 localization
185 (Figure 2F). Indeed, in animals that expresses UNC-116::GFP1-10, CaMKII/UNC-43 is completely absent

bioRxiv preprint doi: https://doi.org/10.1101/2021.09.12.459970; this version posted September 12, 2021. The copyright holder for this preprint (which was not certified by peer review) is the author/funder, who has granted bioRxiv a license to display the preprint in perpetuity. It is made available under aCC-BY-NC 4.0 International license.

from the cell body and strongly accumulates at the axon tip, in contrast to control animals that express GFP1-10 without the kinesin fusion (Figure 2F). Despite this robust redistribution of CaMKII, however, axon degeneration in adult *ric-7(n2657)* animals was not suppressed (Figure 2G). Together with our data showing that overexpressing WT CaMKII has little protection while overexpressing constitutively-active CaMKII strongly suppresses degeneration (Figure 2A), we conclude that CaMKII activity, rather than its localization, is the determinative factor in protecting axons without mitochondria.

CaMKII/UNC-43 suppresses axon degeneration through the conserved Sarm1/TIR-1-ASK1/NSY-1 MAPK pathway

We next sought to identify the downstream targets of CaMKII/UNC-43. In *C. elegans* nervous system, CaMKII/UNC-43 has been shown to regulate asymmetric neural development through the conserved Sarm1/TIR-1-ASK1/NSY-1 MAPK pathway (Chuang and Bargmann, 2005; Hayakawa et al., 2006) (Figure 2H). Specifically, in one of the two AWC sensory neurons, high calcium activates UNC-43, which then directly interacts with TIR-1 and releases the autoinhibition on the TIR domains. Active TIR-1 then recruits and activates the NSY-1 MAPKKK to inhibit the expression of specific odorant receptors. In addition, UNC-43, TIR-1 and NSY-1 colocalize at synaptic regions of AWC and physically interact with each other to form a signaling complex (Chuang and Bargmann, 2005; Sagasti et al., 2001). To test if this signaling complex functions in PVQ degeneration, we examined whether the individual components were required for the protection against degeneration conferred by *unc-43(n498sd)* in animals lacking axonal mitochondria. We found that lof mutations in *tir-1(qd4)* and *nsy-1(ok593)* completely abolish the protection against degeneration conferred by the constitutively active *unc-43(n498sd*) allele (Figure 2I). Thus, the UNC-43/TIR-1/NSY-1 complex functions to suppress axon degeneration in the absence of mitochondria. During development, this complex regulates asymmetric neuronal development via the MAPKK SEK-1 and two redundant P38 MAPKs, PMK-1 and PMK-2 (Alqadah et al., 2016b; Pagano et al., 2015). We could not assess SEK-1 function in axon degeneration, as we found that *ric-7(n2657); sek-1(km4); unc-43(n498sd)* animals are sick and arrest before adulthood, precluding analysis of degeneration. However, we found that loss of PMK-1 alone does not prevent activated CaMKII/UNC-43 from suppressing

bioRxiv preprint doi: https://doi.org/10.1101/2021.09.12.459970; this version posted September 12, 2021. The copyright holder for this preprint (which was not certified by peer review) is the author/funder, who has granted bioRxiv a license to display the preprint in perpetuity. It is made available under aCC-BY-NC 4.0 International license.

degeneration, consistent with the model that redundant PMKs function downstream of the UNC-43/TIR-1/NSY-1 signaling complex (Figure 2I) (Alqadah et al., 2016b; Pagano et al., 2015).

Our data suggest that Sarm1/TIR-1 has an axon protective role: it is required for constitutively activated CaMKII to suppress degeneration due to mitochondria mislocalization (Figure 2I). By contrast, Sarm1/TIR-1 in other contexts—particularly Wallerian degeneration—promotes axon degeneration (Gerdts et al., 2013; Henninger et al., 2016; Osterloh et al., 2012; Turkiew et al., 2017). We examined whether loss of Sarm1/TIR-1 might suppress degeneration in axons that lack mitochondria. We found that neither of the two lof mutations of *tir-1, qd4* and *ok2859*, suppresses PVQ degeneration (Figure 2J). By contrast, overexpression of WT TIR-1 in PVQ strongly suppresses degeneration (Figure 2J). Overall, our results indicate a surprising neuroprotective role for Sarm1/TIR-1 as part of the UNC-43/TIR-1/NSY-1 signaling complex.

Loss of Calsyntenin/CASY-1 suppresses axon degeneration

Our unbiased screen identified a mutation in the *casy-1* gene, *wp60*, that suppresses PVQ degeneration to a similar extent as activated CaMKII/UNC-43 (Figure 3A-3B). CASY-1 is the *C. elegans* homologue of calsyntenin, and comparison of CASY-1 to its *Drosophila* and mammalian homologues shows that these proteins share significant sequence similarity along their entire lengths (Hill et al., 2001). Calsyntenins are type I transmembrane (TM) proteins and are members of the cadherin superfamily (Hill et al., 2001). Their extracellular region contains two cadherin domains and a LG/LNS (laminin G-like) domain and has been shown to regulate synapse development through interactions with neurexin (Kim et al., 2020a; Kim et al., 2020b; Pettem et al., 2013). Their intracellular region is characterized by two kinesin binding sites (KBS), which are important for its anterograde trafficking (Araki et al., 2003; Konecna et al., 2006).

The *C. elegans casy-1* locus encodes three isoforms (Figure 3A). The longest isoform, *casy-1a,* encodes a protein with all domains. The two shorter isoforms, *casy-1b and casy-1c*, share the TM domain and the intracellular region, but do not contain the extracellular cell adhesion domains. The *wp60* allele we identified in the screen is a G-to-A point mutation at the splice acceptor site in the intron before the first kinesin binding site, and it affects all three isoforms (Figure 3A and Figure 1-figure supplement 1D).

bioRxiv preprint doi: https://doi.org/10.1101/2021.09.12.459970; this version posted September 12, 2021. The copyright holder for this preprint (which was not certified by peer review) is the author/funder, who has granted bioRxiv a license to display the preprint in perpetuity. It is made available under aCC-BY-NC 4.0 International license.

We used CRISPR/Cas9 to delete the entire coding region of *casy-1* (Figure 3A and Figure 1-figure supplement 1D). This 11.5kb deletion allele, *wp78*, phenocopies the *wp60* mutation from the screen and strongly suppresses PVQ degeneration (Figure 3B). In the *ric-7(n2657); casy-1(wp78)* animals, PVQ axons rarely degenerate, and only develop a few swellings during the L4-1doa transition (Figure 3C). The phenotype is very similar to the protection conferred by activated CaMKII/UNC-43 (Figure 2B). Further, protection of *casy-1(wp60)* can be abolished by expressing a 34.6kb fosmid that contains the endogenous *casy-1* locus (Figure 3C). Together, these data indicate that loss of calsyntenin/*casy-1* prevents degeneration of axons in *ric-7* animals.

Calsyntenin/CASY-1 TM domain and ICD function together to promote axon degeneration cell autonomously

To determine if CASY-1 acts cell autonomously to promote axon degeneration, we performed PVQ-specific rescue experiments in *ric-7(n2657); casy-1(wp60)* animals, in which degeneration is suppressed due to loss of calsyntenin. Overexpression of full-length calsyntenin completely restored degeneration to *ric-7(n2657); casy-1(wp60)* animals, indicating that calsyntenin is required cell-autonomously for PVQ axon degeneration (Figure 3D). Next, we used this approach to define a minimal fragment of calsyntenin capable of supporting its pro-degeneration function. We examined six CASY-1 fragments (Figure 3D) for their abilities to promote axon degeneration in this context, including the three endogenous isoforms (#1-3, see also Figure 3A), a fragment containing the TM domain + ICD (#4), CASY-1a without the C terminus starting from the first KBS (#5), and the ICD alone (#6). Expression of CASY-1 fragments #1-4, but not #5 or #6, caused strong PVQ degeneration in *ric-7(n2657); casy-1(wp60)* animals (Figure 3D). This structure-function analysis indicated that both calsyntenin's TM domain and the ICD are required for degeneration, while its extracellular region is dispensable. Consistent with these results, we did not observe suppression of degeneration in an existing *casy-1* allele, *tm718,* which is a deletion within the extracellular domain (Figure 3A- 3B).

We then examined if overexpressing *casy-1* promotes degeneration. Overexpressing CASY-1C in *ric-7(n2657); casy-1(wp60)* leads to near complete degeneration at L4, a time point at which only a few *ric-7(n2657)* control animals show degeneration (Figure 3E). However, overexpressing CASY-1C in *casy-*

bioRxiv preprint doi: https://doi.org/10.1101/2021.09.12.459970; this version posted September 12, 2021. The copyright holder for this preprint (which was not certified by peer review) is the author/funder, who has granted bioRxiv a license to display the preprint in perpetuity. It is made available under aCC-BY-NC 4.0 International license.

1(wp60) single mutants does not induce degeneration (Figure 3E). Therefore, overexpressing CASY-1 alone is not sufficient to cause degeneration, but is able to enhance degeneration in the absence of mitochondria.

Anterograde traffic of Calsyntenin/CASY-1 by kinesin promotes axon degeneration

The calsyntenin ICD contains two conserved kinesin binding sites (KBS), and in *C. elegans*, the CASY-1 intracellular region directly binds to kinesin light chain 2 (KLC-2) of the kinesin complex (Ohno et al., 2014). To test the importance of the calsyntenin-KLC interaction for degeneration, we mutated the conserved tryptophan residues in each KBS to alanine (Figure 4-figure supplement 1A) (Konecna et al., 2006). We found that this change completely eliminates the pro-degeneration function of calsyntenin (Figure 4A). These data suggest that calsyntenin functions together with kinesin to mediate degeneration. Next, we tested whether loss of KLC-2 would suppress degeneration, similar to loss of calsyntenin. Indeed, the *klc-2(km11)* lof mutation strongly suppresses degeneration in axons that lack mitochondria (Figure 4B). By contrast, loss of KLC-1 did not affect axon degeneration (Figure 4B). Together, these data suggest that a kinesin complex containing KLC-2 mediates calsyntenin traffic to promote degeneration.

To test this model, we first examined CASY-1's localization in PVQ axons. We used the NATF approach to label endogenous CASY-1 proteins in PVQ. The *gfp11x7* insertion at the C terminus of the endogenous *casy-1* locus does not interfere with CASY-1's pro-degenerative function, as these animals show complete axon degeneration when combined with the *ric-7(n2657)* mutation (Figure 2-figure supplement 1B). Endogenous CASY-1 fluorescence is visible in the PVQ cell body and throughout the axon (Figure 4D). Loss of *ric-7* does not lead to a significant change in steady-state CASY-1 abundance in the cell body or the distal axon (Figure 4D-4F). By contrast, loss of KLC-2 results in a dramatic redistribution of CASY-1 to punctate structures located in the cell body and proximal axon (Figure 4G-4H). This redistribution was accompanied by a near-complete loss of CASY-1 from the distal axon, as well as a partial reduction of CASY-1 levels in the cell body (Figures 4D-4F). The lack of calsyntenin in the distal axon is consistent with a transport defect, while the reduction in the cell body could result from degradation of accumulated CASY-1 in the soma. Together, these data suggest that CASY-1 localization in axons depends on a kinesin complex containing KLC-2.

bioRxiv preprint doi: https://doi.org/10.1101/2021.09.12.459970; this version posted September 12, 2021. The copyright holder for this preprint (which was not certified by peer review) is the author/funder, who has granted bioRxiv a license to display the preprint in perpetuity. It is made available under aCC-BY-NC 4.0 International license.

297 To confirm and extend these results, we performed live imaging. The endogenous CASY-1
298 signals (Figure 4D) were too weak for live imaging of trafficking, so we overexpressed CASY-1C with a C
299 terminal GFP tag. This construct preserves CASY-1's pro-degenerative function, as its expression in *ric-*
300 *7(n2657); casy-1(wp78)* animals leads to strong axon degeneration (Figure 4-figure supplement 1C). Live
301 imaging of CASY-1C::GFP in *casy-1(wp78)* animals show that CASY-1 vesicles undergo extensive
302 trafficking in both the proximal and distal regions of the PVQ axon (Figure 4-figure supplement 1D). We
303 focused on the distal axon region for analysis. Consistent with the previous finding that calsyntenin
304 interacts with kinesin (Steuble et al., 2012), CASY-1C trafficking is highly anterogradely biased (81% of
305 trafficking events are anterograde, Figure 4-figure supplement 1E). For anterograde trafficking, the
306 average speed is 1.07 μm/s, and the average run length is 5.79 μm; for retrograde trafficking, the average
307 speed is 2.08 μm/s, and the average run length is 9.87 μm (Figure 4-figure supplement 1F-1G). Although
308 we found no change in endogenous *casy-1* distribution in *ric-7(n2657)* animals (Figure 4D-4F), we did
309 find that CASY-1C trafficking is greatly affected by *ric-7*: the anterograde bias is largely lost (63% are
310 anterograde), and speeds and run lengths in both directions are dramatically reduced (Figure 4-figure
311 supplement 1F-1G). Overall, the anterograde bias and speed of calsyntenin traffic (Figure 4-figure
312 supplement 1D-1F), together with the dependence of endogenous CASY-1 localization on KLC-2 (Figure
313 4D-4H), demonstrate that *C. elegans* calsyntenin is anterogradely trafficked by kinesin.
314
315 **Mint/LIN-10 is trafficked by calsytenin/CASY-1 and is required for degeneration**
316 Calsyntenin/CASY-1 has been shown to function as a kinesin adaptor that transports vesicular
317 and protein cargoes from the neuronal cell body to the distal axon (Konecna et al., 2006). For example,
318 mammalian calsyntenin-1 can mediate the anterograde transport of APP (Ludwig et al., 2009) and axon
319 guidance receptors such as Robo1 and frizzled 3 (Alther et al., 2016). In *C. elegans*, CASY-1 mediates
320 the translocation of a specific insulin receptor isoform, DAF-2C, from the soma to the distal axon in ASE
321 neurons during taste avoidance learning (Ohno et al., 2014), and also modulates the transport of synaptic
322 vesicles in GABAergic neurons (Thapliyal et al., 2018). It has been proposed that the transport complex
323 consists of four calsyntenin-1 molecules bound to one Kinesin-1 motor (Figure 4-figure supplement 1B)
324 (Ludwig et al., 2009). The intracellular region of calsyntenin, in addition to its kinesin interaction, also

bioRxiv preprint doi: https://doi.org/10.1101/2021.09.12.459970; this version posted September 12, 2021. The copyright holder for this preprint (which was not certified by peer review) is the author/funder, who has granted bioRxiv a license to display the preprint in perpetuity. It is made available under aCC-BY-NC 4.0 International license.

contains a conserved region that has been shown to bind Mint/LIN-10 in mammals (Araki et al., 2003) and an acidic region that has been proposed to buffer calcium (Vogt et al., 2001). To test the importance of the acidic region, we expressed CASY-1C with all the acidic residues in the acidic region mutated to neutral residues (E to Q and D to N). We found that this CASY-1C (mutated acidic) restored strong degeneration to *ric-7(n2657); casy-1(wp60)* animals, but to a lesser extent than the wildtype *casy-1c* transgene (Figure 4A). We conclude that the acidic domain is not essential for calsyntenin's pro-degeneration function; the minor reduction in function may be due to a secondary effect on a different function of this region.

To examine the importance of the Mint/LIN-10 interaction, we tested whether Mint/LIN-10 functions similar to calsyntenin and KLC-2. We found that two independent lof alleles of *lin-10*, *n1853* and *e1439*, suppress axon degeneration (Figure 4C), similar to loss of *casy-1* (Figure 3B). If LIN-10 is a cargo of CASY-1 vesicles, then LIN-10 localization would be affected in *casy-1* KO animals. We labeled endogenous LIN-10 with the NATF approach. In *casy-1(wp78)* single mutants, LIN-10 abundance in the distal axon is dramatically reduced to 56% of the control level, while its abundance in the soma is increased by 27% (Figure 4I-4K). In conclusion, our data suggest a model in which CASY-1 transports LIN-10 from the cell body to the distal axon to mediate axon degeneration in the absence of mitochondria. Since CASY-1C has both a transmembrane sequence and kinesin binding sites, we reasoned that CASY-1C functions as a transmembrane kinesin adaptor that transports Mint/LIN-10 as well as a potential organelle cargo to the distal axon to mediate degeneration (Figure 4-figure supplement 1B).

Loss of calsyntenin/Casy-1 and Mint/LIN-10 suppress axon degeneration through the CaMKII/UNC-43-Sarm1/TIR-1-ASK1/NSY-1 MAPK pathway

We hypothesized that knocking out Calsyntenin/CASY-1 or Mint/LIN-10 protects against degeneration through a specific signaling pathway in axons. It has been shown that Calsyntenin, Mint and APP can form a tripartite complex in mammals (Araki et al., 2003), we thus examined the role of the *C. elegans* APP homologue, APL-1, in spontaneous degeneration in *ric-7(n2657)*. We used the Cre-loxP system to knock out the entire *apl-1* locus in PVQ (Figure 5-figure supplement 1A-1B), but did not observe significant protection against degeneration compared to the P_{PVQ}::Cre control (Figure 5-figure

bioRxiv preprint doi: https://doi.org/10.1101/2021.09.12.459970; this version posted September 12, 2021. The copyright holder for this preprint (which was not certified by peer review) is the author/funder, who has granted bioRxiv a license to display the preprint in perpetuity. It is made available under aCC-BY-NC 4.0 International license.

supplement 1C). We also tested an allele (*wp22*) that deletes most of the APL-1 intracellular region at the C terminus, which has been shown to interact with Mint/LIN-10 (Tomita et al., 1999). *ric-7(n2657); apl-1(wp22)* double mutants still show a complete degeneration phenotype (Figure 5-figure supplement 1C). Therefore, APL-1 is not involved in the spontaneous degeneration in the absence of mitochondria.

Since we identified the *casy-1* and *unc-43* mutations in the same unbiased screen, we next examined the possibility that CaMKII/UNC-43 acts downstream of CASY-1. In *ric-7(n2657); casy-1(wp78)* animals, degeneration is strongly delayed. However, the *unc-43* lof allele *e408* largely abolishes the protection: there is some residual protection in 1doa but degeneration is almost complete in 2doa (Figure 5A). *unc-43(e408)* also suppresses *lin-10(n1853)* and *klc-2(km11)* with a similar trend (Figure 5B-5C). Therefore, the protection against degeneration in *casy-1, lin-10 and klc-2* mutants requires the shared downstream factor CaMKII/UNC-43. We could rescue UNC-43 in *ric-7(n2657); casy-1(wp78); unc-43(e408)* triple mutants by expressing WT or CA UNC-43 in PVQ (Figure 5D), consistent with the cell autonomous role of UNC-43 and CASY-1. We next examined if the TIR-1-NSY-1-SEK-1 signaling also functions downstream of CASY-1. Indeed, the lof mutations, *tir-1(qd4), nsy-1(ok593)* and *sek-1(km4)* all suppress *casy-1(wp78)* (Figure 5E). By contrast, the *pmk-1(km25)* single lof mutation does not suppress *casy-1(wp78)*, consistent with the model that it functions redundantly with other PMKs. Therefore, loss of CASY-1 and LIN-10 acts via the UNC-43-TIR-1-NSY-1 MAPK pathway to protect against axon degeneration in the absence of mitochondria (Figure 5F).

The L-type voltage gated calcium channel subunits EGL-19 and UNC-36 mediate axon protection in *casy-1* and *lin-10* mutants

Our data suggest that loss of CASY-1 and LIN-10 protect axons by activating CaMKII/UNC-43 and its downstream MAP kinase pathway (Figure 5F). How might loss of CASY-1 and LIN-10 increase CaMKII/UNC-43 activity? One possibility is that loss of these factors upregulates CaMKII/UNC-43 abundance in axons in *ric-7(n2657)* mutants. However, endogenous CaMKII/UNC-43 levels in distal PVQ axons are not restored in *ric-7(n2657); casy-1(wp78)* or *ric-7(n2657); lin-10(e1439)* animals compared to the *ric-7(n2657)* control (Figure 6-figure supplement 1). Therefore, CASY-1 and LIN-10 do not regulate CaMKII/UNC-43 protein levels in axons. We next tested the hypothesis that loss of CASY-1 or LIN-10

bioRxiv preprint doi: https://doi.org/10.1101/2021.09.12.459970; this version posted September 12, 2021. The copyright holder for this preprint (which was not certified by peer review) is the author/funder, who has granted bioRxiv a license to display the preprint in perpetuity. It is made available under aCC-BY-NC 4.0 International license.

may alter CaMKII/UNC-43 activity by regulating calcium homeostasis. We focused on the voltage-gated calcium channels (VGCC) for two reasons: first, calcium influx through VGCCs can activate CaMKII/UNC-43 (Sagasti et al., 2001; West et al., 2001); second, Mint/LIN-10 has been shown to directly interact with VGCCs in mammals (Maximov and Bezprozvanny, 2002; Maximov et al., 1999).

In *C. elegans*, the L-type VGCC α_1 subunit, EGL-19, the Non-L-type α_1 subunit, UNC-2, and the regulatory $\alpha_2\delta$ subunit, UNC-36, have been shown to function upstream of CaMKII/UNC-43 (Alqadah et al., 2016a; Alqadah et al., 2016b; Caylor et al., 2013; Sagasti et al., 2001). We thus examined if these subunits are required for protection against axon degeneration in *casy-1* and *lin-10* mutants. We found that the lof mutations *egl-19(n582)* and *unc-36(e251)* completely abolish the delayed degeneration in adult *ric-7(n2657); casy-1(wp78)* animals (Figure 6A-6B). They also suppress the protection in *ric-7(n2657); lin-10(n1853*) animals, with *ric-7(n2657); lin-10(n1853); egl-19(n582)* triple mutants also displaying enhanced degeneration at L4 (Figure 6C-6D). By contrast, the lof mutation *unc-2(e55)* does not suppress *casy-1(wp78)*, and partially suppresses *lin-10(n1853)* (Figure 6-figure supplement 2A-2B). We conclude that the L-type VGCC composed of EGL-19 and UNC-36 is required for axon protection in *casy-1* and *lin-10* mutants.

Next, we determined the relationship of the EGL-19/UNC-36 calcium channel to CaMKII/UNC-43 in axon protection. We found that the EGL-19/UNC-36 calcium channel is not required for protection conferred by gain-of-function in CaMKII/UNC-43: *unc-36(e251*); *ric-7(n2657); unc-43(n498sd)* animals are protected from axon degeneration similar to *ric-7(n2657); unc-43(n498sd)* alone (Figure 6E). These data indicate that CaMKII/UNC-43 activity acts downstream of EGL-19/UNC-36 calcium channel, consistent with the model that VGCCs act to activate CaMKII/UNC-43 (Alqadah et al., 2016b). Importantly, we found that while EGL-19, UNC-36, and CaMKII/UNC-43 are required to suppress degeneration triggered by loss of mitochondria, loss of any of these factors is not sufficient to trigger axon degeneration in otherwise wild-type animals (Figure 6-figure supplement 2C). Thus, the VGCC-CaMKII/UNC-43 pathway is required specifically for axon protection conferred by loss of *casy-1* or *lin-10* in the context of mitochondria mislocalization. Overall, our data suggest a model in which loss of CASY-1 or LIN-10 results in increased neuronal calcium via L-type VGCC. Increased calcium leads to activation of CaMKII/UNC-43. In turn,

bioRxiv preprint doi: https://doi.org/10.1101/2021.09.12.459970; this version posted September 12, 2021. The copyright holder for this preprint (which was not certified by peer review) is the author/funder, who has granted bioRxiv a license to display the preprint in perpetuity. It is made available under aCC-BY-NC 4.0 International license.

CaMKII/UNC-43 activity suppresses axon degeneration through the TIR-1-NSY-1-SEK-1 MAPK pathway (Figure 6F).

The calsyntenin-CaMKII-MAPK pathway protects against early-stage degeneration, before axon breakage

Axon degeneration is a sequence of events beginning with axon thinning/beading, followed by axon breakage, fragmentation and ending with debris clearance (Figure 1H). At what step does the calsyntenin-CaMKII-MAPK pathway prevent degeneration? To test whether the calsyntenin-CaMKII-MAPK pathway can prevent the late steps of degeneration that occur after axon breakage, we used laser axotomy to experimentally induce an axon break in one PVQ axon and examined the degeneration of the distal axon segment 24 hours later. Consistent with previous findings (Ding and Hammarlund, 2018; Nichols et al., 2016; Rawson et al., 2014), injury-induced degeneration of distal PVQ axon segments is slow, as nearly all axons are still present 24 hours later (Figure 1-figure supplement 2A-2B). By contrast, in *ric-7(n2657)* mutants, degeneration after injury is greatly enhanced due to the lack of axonal mitochondria (Figure 1-figure supplement 2A-2B) (Ding and Hammarlund, 2018; Nichols et al., 2016; Rawson et al., 2014). However, loss of calsyntenin or activation of CaMKII did not significantly suppress degeneration in *ric-7(n2657)* after axon transection (Figure 1-figure supplement 2B). These data indicate that the calsyntenin-CaMKII-MAPK pathway protects against degeneration by acting before axon breakage, and cannot stop degeneration after axon breaks occur. Consistent with this model, protected axons in *ric-7(n2657); casy-1(wp78)* and *ric-7(n2657); unc-43(n498sd)* animals mostly stop at the beading stage, and rarely enter the breaking stage (Figure 2B and 3C). Therefore, we conclude that the calsyntenin-CaMKII-MAPK pathway specifically prevents the transition from axon thinning and beading towards axon breakage.

Discussion

bioRxiv preprint doi: https://doi.org/10.1101/2021.09.12.459970; this version posted September 12, 2021. The copyright holder for this preprint (which was not certified by peer review) is the author/funder, who has granted bioRxiv a license to display the preprint in perpetuity. It is made available under aCC-BY-NC 4.0 International license.

Axon degeneration is a critical step in neurodegenerative disease. We used an unbiased approach to identify mechanisms that regulate axon degeneration triggered by loss of axonal mitochondria. We discovered a novel anti-degenerative pathway involving CaMKII/UNC-43, Sarm1/TIR-1, and MAP kinase signaling. In particular, constitutively active CaMKII/UNC-43 activates Sarm1/TIR-1 and the downstream NSY-1-SEK-1 MAPK pathway to protect against degeneration in a cell-specific manner. Furthermore, we found that the loss of the conserved calsyntenin/Mint/KLC-2 trafficking complex activates the CaMKII-TIR-1-MAPK pathway through the L-type VGCC and suppresses degeneration.

A key anti-degenerative role for CaMKII

We discovered that CaMKII/UNC-43 is a key factor in regulating axon degeneration when mitochondria are absent. CaMKII is an abundant kinase that is well studied in neurons. Calcium sensitivity is conferred by the interaction with Ca^{2+}/calmodulin. Binding of Ca^{2+}/calmodulin releases the autoinhibition of CaMKII and activates the enzyme (Lisman et al., 2002). CaMKII can also undergo autophosphorylation, leading to persistent activation even after dissociation of calmodulin (Lisman et al., 2002). CaMKII in neurons is well studied for its role in long-term potentiation (LTP), which is one of the major mechanisms underlying learning and memory (Lisman et al., 2002). Ca^{2+} entry into postsynaptic sites activates CaMKII, which then initiates the signaling cascades that potentiate synaptic transmission (Lisman et al., 2002). CaMKII is enriched at postsynaptic density (PSD), and interacts with numerous PSD proteins, including NMDA receptor, AMPA receptor, F-actin and calcium channels to regulate synaptic function (Hell, 2014; Lisman et al., 2002; Zalcman et al., 2018). Besides its role in learning and memory, neuronal CaMKII has been proposed to function in neurodegeneration, although its role has been unclear. On the one hand, CaMKII has a pro-degenerative function in the context of calcium overload. For example, CaMKII promotes axon degeneration downstream of a mutant TRPV4 channel, where it acts to increase intracellular Ca^{2+} (Woolums et al., 2020). On the other hand, in the *Drosophila* retina, failure to activate CaMKII leads to photoreceptor cell death (Alloway et al., 2000; Kristaponyte et al., 2012). Consistent with a function in opposing cell death, it was recently shown that activation of CaMKII in mouse retinal ganglion cells protects them against cell death induced by excitotoxicity, optic nerve injury and glaucoma models (Guo et al., 2021). Here, we show that in axon degeneration caused

bioRxiv preprint doi: https://doi.org/10.1101/2021.09.12.459970; this version posted September 12, 2021. The copyright holder for this preprint (which was not certified by peer review) is the author/funder, who has granted bioRxiv a license to display the preprint in perpetuity. It is made available under aCC-BY-NC 4.0 International license.

463 by the absence of mitochondria, CaMKII/UNC-43 acts to oppose axon degeneration: its activation
464 strongly suppresses axon degeneration cell autonomously.

465 Our data indicate that CaMKII's effect on axon degeneration is context dependent. Loss of
466 CaMKII/UNC-43 alone does not affect axon stability, as the *unc-43(e408)* single mutants do not show
467 spontaneous axon degeneration (Figure 2A). However, in the context of axonal mitochondria depletion,
468 loss of CaMKII accelerates degeneration, while CaMKII activation is neuroprotective. Loss of axonal
469 mitochondria also reduces axonal levels of CaMKII (Figure 2D and 2E). Together, these observations
470 suggest that reduced axonal CaMKII activity contributes to degeneration. However, since even complete
471 loss of CAMKII does not trigger degeneration when axonal mitochondria are normal, loss of axonal
472 mitochondria must trigger parallel pro-degenerative signals besides having effects on CaMKII. This is not
473 surprising since mitochondria perform multifaceted activities to regulate neuronal metabolism.
474 Nonetheless, our work reveals that active CaMKII/UNC-43 can protect against axon degeneration in the
475 absence of mitochondria, which may serve as an entry point for therapeutical interventions.
476

477 **CaMKII localization and activation depend on mitochondria**

478 We observed that loss of axonal mitochondria results in reduced axonal CaMKII/UNC-43,
479 suggesting that axonal CaMKII localization or stabilization depends on mitochondria. Precise control of
480 CaMKII localization in neurons is critical for its function. For example, although CaMKII is highly abundant
481 throughout neuronal processes, anchoring at dendritic spines refines its substrate selectivity and is
482 important for LTP (Hell, 2014). It has been well studied that CaMKII can translocate to PSD upon
483 stimulation (Otmakhov et al., 2004; Shen and Meyer, 1999), and the translocation involves interactions
484 with PSD proteins such as NMDA receptors (Halt et al., 2012; Merrill et al., 2005). However, the
485 mechanisms governing CaMKII transport and abundance in axons are unclear. In *C. elegans*,
486 translocation of CaMKII/UNC-43 to neurites has been shown to be regulated by the interactions between
487 the catalytic and autoinhibitory domain (Umemura et al., 2005). Multiple mutations that mimic
488 autophosphorylation result in an increased neurite pool of CaMKII/UNC-43. It has been proposed that
489 unknown transport factors facilitate the trafficking of CaMKII/UNC-43 by binding to its catalytic domain,
490 and conformational changes of CaMKII/UNC-43 affect the interactions with the transport factors

bioRxiv preprint doi: https://doi.org/10.1101/2021.09.12.459970; this version posted September 12, 2021. The copyright holder for this preprint (which was not certified by peer review) is the author/funder, who has granted bioRxiv a license to display the preprint in perpetuity. It is made available under aCC-BY-NC 4.0 International license.

(Umemura et al., 2005). In this study, we show that axonal mitochondria are important for endogenous CaMKII/UNC-43 localization in axons. It is possible that some CaMKII/UNC-43 transport factors are present on mitochondria, thus facilitating co-trafficking into axons.

In addition to reduced levels of axonal CaMKII/UNC-43, our data indicate that loss of axonal mitochondria also results in deficient CaMKII/UNC-43 activation. Overexpression of WT CaMKII/UNC-43 in *ric-7* animals has only a small protective effect on degeneration (Figure 2A). By contrast, mutations that activate endogenous CaMKII, or overexpression of the activated form, strongly suppress degeneration (Figure 2A). Thus, CaMKII activation is a key choke point in the ability of axons to withstand degeneration. One possibility is that mitochondria can act as activators of CaMKII/UNC-43 through modulating local calcium homeostasis in axons. Overexpression of calcium-independent constitutively-active (CA) CaMKII/UNC-43 can thus strongly suppresses degeneration, even though axonal mitochondria are absent.

A calsyntenin/Mint/kinesin trafficking complex controls CaMKII activity and degeneration

We also found that PVQ neurons lacking calsyntenin/CASY-1 are highly resistant to degeneration. Calsyntenins are a family of neuronally enriched transmembrane (TM) proteins characterized by the presence of two cadherin-like repeats, a LG/LNS domain in the extracellular region and an intracellular domain (ICD) that carries two kinesin binding sites (KBS) (Araki et al., 2003; Konecna et al., 2006). The three human calsyntenin proteins (CLSTN1-3) regulate diverse neuronal functions. For example, CLSTN1 mediates trafficking of NMDA receptors (Ster et al., 2014) and axon guidance receptors (Alther et al., 2016), and regulates axon branching (Ponomareva et al., 2014) and microtubule polarity (Lee et al., 2017). CLSTN2 is involved in learning and memory (Lipina et al., 2016; Preuschhof et al., 2010). CLSTN3 has been shown to mediate synapse development (Pettem et al., 2013). Previous studies have also associated calsyntenins with neurodegeneration, specifically Alzheimer's disease pathogenesis (Gotoh et al., 2020; Uchida and Gomi, 2016; Vagnoni et al., 2012). There is also evidence for functional mammalian calsyntenins without the extracellular domain. For example, mammalian calsyntenins undergo proteolytic cleavage by α-secretase to produce the membrane-bound C-terminal fragment (CTF), which can be further cleaved by γ-secretase to produce the cytosolic ICD (Araki et al.,

bioRxiv preprint doi: https://doi.org/10.1101/2021.09.12.459970; this version posted September 12, 2021. The copyright holder for this preprint (which was not certified by peer review) is the author/funder, who has granted bioRxiv a license to display the preprint in perpetuity. It is made available under aCC-BY-NC 4.0 International license.

519 2004; Hata et al., 2009; Vogt et al., 2001). Calsyntenin CTF and ICD have been shown to regulate the
520 trafficking, metabolism and signaling of amyloid precursor protein (APP) (Araki et al., 2007; Araki et al.,
521 2004; Araki et al., 2003; Steuble et al., 2012; Takei et al., 2015). In addition, a recent study shows that
522 mouse calsyntenin 3β, which lacks the extracellular region for cell adhesion, promotes the secretion of
523 S100b from brown adipocytes and stimulates sympathetic innervation (Zeng et al., 2019).
524 We show that in the absence of mitochondria, the CASY-1 TM domain and ICD function as a
525 kinesin adaptor to mediate degeneration. Specifically, the interaction between CASY-1's kinesin-binding
526 sites and the kinesin light chain KLC-2 is critical for its pro-degenerative function (Figure 4A). Further, loss
527 of *klc-2,* like loss of calsyntenin, suppresses degeneration (Figure 4B). The *C. elegans* genome encodes
528 two kinesin light chain genes, *klc-1* and *klc-2*. However, loss of *klc-1* did not phenocopy the *casy-1* or *klc-*
529 *2* mutant (Figure 4B). Consistent with these data, *klc-1* does not appear to be expressed in PVQ (Taylor
530 et al., 2020). Further, KLC-1 is a divergent kinesin and its function in axonal transport is unclear
531 (Sakamoto et al., 2005), Thus, calsyntenin specifically acts with the kinesin light chain KLC-2 to mediate
532 axon degeneration. We also found that loss of the calsyntenin/CASY-1 cargo, Mint/LIN-10, suppresses
533 degeneration (Figure 4C). Therefore, our data support a model in which disruption of a
534 calsyntenin/Mint/KLC-2 trafficking complex prevents axon degeneration in the absence of mitochondria.
535
536 **L-type calcium channels link the calsyntenin/Mint/KLC-2 trafficking complex to CaMKII activity**
537 **and axon protection**
538 We found that axon protection by loss of calsyntenin or Mint requires L-type voltage-gated
539 calcium channels (VGCC). VGCCs are composed of a pore-forming α_1 subunit, and are usually
540 associated with auxiliary β subunits and α2δ subunits (Catterall, 2011). In *C. elegans* EGL-19 is the L-
541 type α_1 subunit, and UNC-36 is the $\alpha_2\delta$ subunit (Hobert, 2013). L-type VGCCs composed of EGL-19 and
542 UNC-36 have critical roles in neurons in calcium influx (Frokjaer-Jensen et al., 2006). However, L-type
543 VGCCs have not been previously shown to mediate neurodegeneration. We found that loss of *egl-19* or
544 *unc-36* completely blocks the protective effect of disrupting the calsyntenin/Mint/KLC-2 trafficking complex
545 (Figure 6A-6D). As L-type channels are known to bind Mint, these data suggest that disrupting the

bioRxiv preprint doi: https://doi.org/10.1101/2021.09.12.459970; this version posted September 12, 2021. The copyright holder for this preprint (which was not certified by peer review) is the author/funder, who has granted bioRxiv a license to display the preprint in perpetuity. It is made available under aCC-BY-NC 4.0 International license.

546 calsyntenin/Mint/KLC-2 trafficking complex changes the localization of L-type calcium channels. In turn,
547 reorganized calcium channels protect axons.

548 What is the target of reorganized calcium channels? In *C. elegans*, EGL-19 and UNC-36 have
549 been shown to activate CaMKII/UNC-43 (Alqadah et al., 2016a; Alqadah et al., 2016b; Caylor et al., 2013;
550 Sagasti et al., 2001). In mammals, L-type channels can act as CaMKII anchor proteins at postsynaptic
551 sites and allow efficient CaMKII stimulation upon Ca^{2+} influx (Abiria and Colbran, 2010; Hudmon et al.,
552 2005; Rose et al., 2009). We found that L-type calcium channels are not required for axon protection by
553 activated CaMKII (Figure 6E). These data suggest that a key result of reorganized calcium channels is
554 the activation of CaMKII. If CaMKII is activated by a gain of function mutation, its activity is not dependent
555 on calcium and does not require reorganized L-type channels. The loss of the calsyntenin/Mint/KLC-2
556 trafficking complex may enhance signaling from L-type calcium channels to CaMKII by regulating channel
557 localization, channel abundance on the membrane, or channel association with CaMKII.

558 It is interesting to speculate that loss of calsyntenin activates the CaMKII-TIR-1-MAPK pathway
559 through the L-type VGCC in distal axons. The evidence supporting the local effects are: 1, CaMKII/UNC-
560 43 abundance is reduced specifically in distal axons in the absence of mitochondria; 2, delivery of
561 calsyntenin and Mint by kinesin into distal axons is important for degeneration; 3, Mint/LIN-10,
562 CaMKII/UNC-43, Sarm1/TIR-1 and NSY-1 have been shown to colocalize at synaptic regions in distal
563 axons (Chuang and Bargmann, 2005), and L-type VGCCs are enriched at postsynaptic sites (Hell et al.,
564 1996); 4, spontaneous degeneration only happens in distal axons but never affects cell bodies and
565 proximal axons. However, our data do not exclude the possibility that CaMKII/UNC-43 is activated in cell
566 bodies to suppress degeneration. Even if activation takes place in the distal axon, activated MAP kinases
567 may eventually deliver axon-protective activity to the cell body by retrograde transport. Further
568 experiments that examine CaMKII/UNC-43 and MAPK activity in distinct compartments will help
569 disentangle these two models.

570

571 **The surprising neuroprotective role of the Sarm1/TIR-1-ASK1/NSY-1 MAPK pathway**

572 We discovered a surprising axon-protective role of the *C. elegans* Sarm1 homologue, TIR-1.
573 Sarm1 was initially identified as an essential activator of injury-induced axon degeneration in flies and

bioRxiv preprint doi: https://doi.org/10.1101/2021.09.12.459970; this version posted September 12, 2021. The copyright holder for this preprint (which was not certified by peer review) is the author/funder, who has granted bioRxiv a license to display the preprint in perpetuity. It is made available under aCC-BY-NC 4.0 International license.

mammals (Gerdts et al., 2013; Osterloh et al., 2012). Sarm1 promotes axon degeneration by regulating NAD^+ metabolism (Essuman et al., 2017; Gerdts et al., 2015). Specifically, the TIR domain possesses intrinsic capabilities to hydrolyze NAD^+, but its activity is normally autoinhibited by the ARM domain in healthy axons (Essuman et al., 2017). Upon axon injury, the autoinhibition is released, causing rapid NAD^+ collapse, which eventually leads to axon degeneration. Sarm1 was later shown to mediate other types of axon degeneration such as in traumatic brain injury (Henninger et al., 2016) and peripheral neuropathy (Turkiew et al., 2017). Interestingly, there is evidence for Sarm1 involvement in neurodegeneration downstream of drug-induced mitochondria dysfunction (Loreto et al., 2020; Summers et al., 2014; Summers et al., 2020). However, other forms of neurodegeneration, such as SOD1-ALS, do not require Sarm1 (Peters et al., 2018), indicating that multiple pro-degeneration mechanisms may exist. *C. elegans* Sarm1 is well conserved with its counterparts in other species, containing Armadillo/HEAT (ARM) repeat domains, two sterile alpha motifs (SAM), and a Toll/interleukin-1 receptor homology (TIR) domain. Further, activated *C. elegans* TIR domains have been shown to cause NAD^+ depletion and trigger axon degeneration in cultured mouse neurons (Summers et al., 2016). Therefore, the capacity to deplete NAD^+ and promote axon degeneration is likely conserved in CeTIR-1. However, so far, there is little evidence that the NAD^+ hydrolase activity of CeTIR-1 is essential to axon degeneration in *C. elegans in vivo*. Loss of CeTIR-1 does not protect against axon degeneration induced by laser axotomy in *C. elegans* (Nichols et al., 2016). Overexpressing the murine Wld^S or the *C. elegans* Nmnats, which promote NAD^+ synthesis, does not delay axon degeneration (Nichols et al., 2016). Our data show that spontaneous axon degeneration caused by the loss of mitochondria does not require CeTIR-1. Together these data suggest that NAD^+ consumption by CeTIR-1 does not play an essential role in promoting axon degeneration in *C. elegans*.

Quite unexpectedly, we found that Sarm/TIR-1 activity is required for the protection against axon degeneration by active UNC-43/CaMKII, and this protection is mediated by the conserved NSY-1-SEK-1 MAPK pathway. In general, Sarm/TIR-1 family members have a complex relationship with MAP kinase signaling. Sarm1 has been shown to coordinate with different MAP kinase components to promote axon degeneration in mammals. Specifically, the MAPKKKs MEKK4, MLK2, and DLK, the MAPKKs MKK4 and MKK7, and the MAPKs JNK1-3 are required for axon degeneration after injury (Walker et al., 2017; Yang

bioRxiv preprint doi: https://doi.org/10.1101/2021.09.12.459970; this version posted September 12, 2021. The copyright holder for this preprint (which was not certified by peer review) is the author/funder, who has granted bioRxiv a license to display the preprint in perpetuity. It is made available under aCC-BY-NC 4.0 International license.

et al., 2015). However, an *in vivo* study in *Drosophila* did not observe the involvement of JNK in injury-induced axon degeneration (Neukomm et al., 2017). The NSY-1-SEK-1 pathway is a different MAPK cascade: NSY-1(MAPKKK) is the homologue of human ASK1(or MEKK5), SEK-1(MAPKK) is the homologue of human MKK3/6, and the downstream MAPKs are PMKs, which fall in the p38 rather than the JNK family (Hayakawa et al., 2006). The discrepancy between the neuroprotective role that we observed here and the previously identified pro-degenerative role of the TIR-1-MAPK pathways may be due to the specificity of the MAPK pathways that are activated in these different contexts. It is possible that distinct MAPK pathways are activated during different types of degeneration, and function through distinct downstream factors. It has been well established that the TIR-1-NSY-1-SEK-1-PMK-1 signaling acts in innate immunity to resist bacterial pathogens (Kim et al., 2002). The pathway also functions in the nervous system to regulate asymmetric neural development, with PMK-1 and PMK-2 acting redundantly (Alqadah et al., 2016b; Pagano et al., 2015). Interestingly, a previous study has shown that this pathway promotes motor neuron degeneration in a *C. elegans* model of ALS (Veriepe et al., 2015). In these animals, secreted molecules from neurons that overexpress human TDP-43 or FUS activates the transcription factor ATF-7 through the TIR-1-MAPK pathway and leads to neurodegeneration. Here, PMK-1 and ATF-7 form a linear pathway downstream of SEK-1 to mediate degeneration. However, in our *ric-7(n2657)* model, loss of PMK-1 does not abolish the protection against degeneration, suggesting that redundant MAPKs and potentially different downstream effectors are involved. It would be helpful to identify these factors in further research in order to fully delineate the neuroprotective pathway.

An active mechanism that overrides neurodegeneration

Mitochondria defects are tightly associated with neurodegeneration. Because lack of axonal mitochondria results in completely penetrant PVQ axon degeneration, this model offers an opportunity to discover cellular mechanisms that control degeneration. This work identifies a linear CaMKII/UNC-43-Sarm1/TIR-1-ASK1/NSY-1 MAPK pathway as an active neuroprotective program that suppresses axon degeneration due to loss of axonal mitochondria. The surprising protective role of these molecules in this context highlights the complex nature of axon degeneration. In contexts where axon degeneration is

bioRxiv preprint doi: https://doi.org/10.1101/2021.09.12.459970; this version posted September 12, 2021. The copyright holder for this preprint (which was not certified by peer review) is the author/funder, who has granted bioRxiv a license to display the preprint in perpetuity. It is made available under aCC-BY-NC 4.0 International license.

629 associated with defects in mitochondria location or function, the calsyntenin-CaMKII-MAPK pathway may

630 provide intervention points for suppressing degeneration.

bioRxiv preprint doi: https://doi.org/10.1101/2021.09.12.459970; this version posted September 12, 2021. The copyright holder for this preprint (which was not certified by peer review) is the author/funder, who has granted bioRxiv a license to display the preprint in perpetuity. It is made available under aCC-BY-NC 4.0 International license.

Materials and Methods

C. elegans

Worms were maintained at 20°C on NGM plates seeded with OP50 *E. coli*. Hermaphrodites were used for all the assays in this study. Worm strains in this study are listed in the Key Resources Table.

Generation of transgenic worms and CRISPR

Transgenic animals were generated by microinjection with Promega 1kb DNA ladder as a filler in the injection mix. Plasmids for injection were assembled using Gateway recombination (Invitrogen). Entry clones for Gateway reactions were generated by Gibson Assembly (Gibson et al., 2009).

CRISPR/Cas9 was used to generate deletions and knock-ins according to a recent improved protocol (Ghanta and Mello, 2020). Briefly, 0.5µl of 10µg/ul Cas9 protein was mixed with 5µl of 0.4µg/ul tracrRNA and 2.8µl of 0.4µg/µl crRNA from IDT and was incubated @ 37°C for 15 minutes. Then 25ng/µl double-stranded DNA donor with 40-50 bp homology arms was added to the mixture. 1.6µl of 500ng/µl PRF4::*rol-6(su1006)* plasmid was also added as a selection marker (Mello et al., 1991). Nuclease free water was added to bring the final volume to 20µl. The mixture was then centrifuged @ 15,000rpm for 2min. 16µl of the mixture was transferred to a fresh tube and was kept on ice before injection. To increase the frequency of homology-directed repair, the dsDNA donor amplified by PCR was melted and cooled before use according to the protocol (Ghanta and Mello, 2020). F1 non-rollers were then selected for genotyping to find heterozygous mutants. Homozygotes were sequenced to confirm the edits. crRNAs, genotyping primers and repair templates can be found in Table 1.

The *casy-1::gfp11x7* KI strain PHX3311 was generated by SunyBiotech using CRISPR/Cas9 with two guide RNAs simultaneously (See Table 1).

Table 1: List of key oligonucleotides for CRISPR

Name	Sequence	Source
crRNA(20bp immediately 5' to the PAM sequence)		
casy-1(wp78) 5'	gtgagggtggaaaatgattg	IDT

bioRxiv preprint doi: https://doi.org/10.1101/2021.09.12.459970; this version posted September 12, 2021. The copyright holder for this preprint (which was not certified by peer review) is the author/funder, who has granted bioRxiv a license to display the preprint in perpetuity. It is made available under aCC-BY-NC 4.0 International license.

casy-1(wp78) 3'	tgtgatgtaatcaacagggt	IDT
unc-43-gfp11x7	gagaaaaataggcataaaga	IDT
casy-1-gfp11x7#1	agaacgagcgttcgttgaga	SunyBiotech
casy-1-gfp11x7#2	tgtcgttggaggtcttgagt	SunyBiotech
lin-10-gfp11x7	ataaacaatcaaatgtattg	IDT
genotyping primers		
casy-1(wp78)	f: gaataagaatgagaagacccgctgc; r1: ctccttgcagattgattattggcgc; r2: aaggagtgaaaaggacagtatgaagacg	IDT
unc-43-gfp11x7	f: tcagaaacggagaagctcatacccg; r1: tcatgtagtaccatatggtcgcgtcc; r2: ccatatatctgagagaatgggacaag	IDT
casy-1-gfp11x7	f: aaattccttcaggcatgttg; r: gaaggagtgaaaaggacagt	IDT
lin-10-gfp11x7	f: tcgcagttgcacatgacaggtgag; r: attcacattagggcgcactttctgg	IDT
Others		

bioRxiv preprint doi: https://doi.org/10.1101/2021.09.12.459970; this version posted September 12, 2021. The copyright holder for this preprint (which was not certified by peer review) is the author/funder, who has granted bioRxiv a license to display the preprint in perpetuity. It is made available under aCC-BY-NC 4.0 International license.

7XGFP11 template	tcaggaggccgtgaccacatggtccttcatgagtatgtaaatgctgctgggattacaggtg gctctggaggtagagatcatatggttctccacgaatacgttaacgccgcaggcatcactgg cggtagtggaggacgcgaccatatggtactacatgaatatgtcaatgcagccggaataac cggagggtccggaggccgggatcacatggtgctgcatgagtatgtgaacgcggcgggtat aactggtgggtcgggcggacgagaccatatggtgcttcacgaatacgtaaacgcagctgg cattactggcggatcaggtggcagggatcacatggtactccatgagtacgtgaacgctgct ggaatcacaggcggtagcggcggtcgggaccatatggtcctgcacgaatatgtcaatgct gccggtatcaccggcggcaag	IDT
GFP1-10 template	atgtccaaaggagaagaactgtttacgggtgttgtgccaattttggttgaactcgatggtga tgtcaacggacataagttctcagtgagaggcgaaggagaaggtgacgccaccattggaa aattgactcttaaattcatctgtactactggtaaacttcctgtaccatggccgactctcgtaa caacgcttacgtacggagttcagtgcttttcgagatacccagaccatatgaaaagacatga ctttttttaagtcggctatgcctgaaggttacgtgcaagaaagaacaatttcgttcaaagatg atggaaaatataaaactagagcagttgttaaatttgaaggagatactttggttaaccgcat tgaactgaaaggaacagattttaaagaagatggtaatattcttggacacaaactcgaata caattttaatagtcataacgtatacatcactgctgataagcaaaagaacggaattaaagcg aatttcacagtacgccataatgtagaagatggcagtgttcaacttgccgaccattaccaac aaaacacccctattggagacggtccggtacttcttcctgataatcactacctctcaacacaa acagtcctgagcaaagatccaaatgaaaaataa	IDT

654

655 ## Fosmid preparation

656 The bacteria clone that contains the WRM0622dH03 fosmid was grown overnight in 3ml LB with
657 1.1µl chloramphenicol. 6µl 500X CopyControl Fosmid Autoinduction Solution was also added to induce

bioRxiv preprint doi: https://doi.org/10.1101/2021.09.12.459970; this version posted September 12, 2021. The copyright holder for this preprint (which was not certified by peer review) is the author/funder, who has granted bioRxiv a license to display the preprint in perpetuity. It is made available under aCC-BY-NC 4.0 International license.

658 the fosmid to high copy according to the CopyControl Fosmid Library Production Kits (EPICENTRE). The
659 fosmid was then prepared using the standard Qiagen miniprep kit.
660
661 ## Quantification of axon degeneration
662 Worms at the desired age were immobilized with 10mM levamisole in M9 and mounted on a 3%
663 agarose pad on a glass slide. Worms were then examined under a Zeiss Axioplan 2 microscope
664 equipped with a Zeiss Plan-APROCHROMAT 63X/1.4 oil objective and a pE-300 LED from CoolLED.
665 Fractions of worms with two non-truncated (intact) PVQ axons were quantified.
666
667 ## *ric-7* suppressor screen and mapping
668 *XE2046(oyIs14[sra-6p::GFP], ric-7(n2657) V)* worms were mutated with 47mM EMS. Three F1s
669 were placed on each plate. We screened around 50 F2 adults from each plate using a Zeiss Axioplan 2
670 microscope with a Zeiss 63X/1.4 oil objective. A total of 340 plates were screened. Animals with strong
671 suppression of PVQ truncation was recovered. The suppression phenotype was further confirmed in the
672 following generations.
673 Mutants from the screen were backcrossed with the parent strain *XE2046(oyIs14[sra-6p::GFP],*
674 *ric-7(n2657) V)* three to four times. Genomic DNA were extracted using Phenol/$CHCl_3$ extraction from the
675 backcrossed worms. Briefly, 10 plates of freshly starved worms were collected with M9, washed and
676 centrifuged to obtain ~100µl pellet. The pellet was then lysed with 350µl lysis buffer (50mM KCl, 10mM
677 Tris pH 8.3, 25mM MgCl2, 0.45% Nonidet P-40, 0.45% Tween-20 and 0.01% gelatin), 12µl 20% SDS, 2µl
678 20mg/ml proteinase K and 1µl β-mercaptoethanol at 65°C (water bath) for 2 hours. Next, 235µl lysis
679 buffer was added to bring the final volume to 700µl. 700µl of Phenol/$CHCl_3$ was then added and mixed
680 with the lysate. The solution was left resting for 1min until both phases were defined. The tube was
681 centrifuged for 5min at 15,000rpm at room temperature. 500µl supernatant was transferred to a new tube
682 and another round of Phenol/CHCl3 was performed to get 400 µl supernatant. Ethanol/NaOAc
683 precipitation was then performed by adding 50µl 3M NaOAc (1:10) and 1,250µl 100% ice cold ethanol
684 (2.5 volumes) and incubating on ice for 10min. Precipitated nucleic acids and salts were spun down at
685 4°C and the supernatant was removed. 400µl EB buffer was added and the tube was incubated at 37°C

bioRxiv preprint doi: https://doi.org/10.1101/2021.09.12.459970; this version posted September 12, 2021. The copyright holder for this preprint (which was not certified by peer review) is the author/funder, who has granted bioRxiv a license to display the preprint in perpetuity. It is made available under aCC-BY-NC 4.0 International license.

(water bath) for 10min to dissolve the DNA. 2.3µl P1 buffer from the Qiagen miniprep kit that contains RNAse was then added and the tube was incubated at 37°C (water bath) for 30min to remove RNA. Another round of Phenol/CHCl3 extraction was performed to get 400µl supernatant. Then Ethanol/NaOAc precipitation was done to obtain the DNA pellet. The pellet was washed with 70% ice cold ethanol 3 times to remove salts. The pellet was then air dried for 10min and dissolved in 50µl nuclease-free water at 37°C overnight. The DNA concentration was then measured and examined by electrophoresis the next day. The final genomic DNA were sent for whole genome sequencing at the Yale Center for Genome Analysis. The parent strain was also sequenced as the control. Sequencing was performed using NovaSeq S4 paired-end 150bp with each sample taking up 1.5% of a lane. The final coverage was around 70-150x.

Sequencing results were analyzed using MiModD (Maier and Baumeiste, 2016) on the galaxy server (Afgan et al., 2016). Briefly, reads were aligned to the reference genome (the WS220/ce10 assembly) using Bowtie2 (Langmead and Salzberg, 2012). Homozygous variants in each mutant strain were then extracted based on the same reference genome using mimodd_varcall and mimodd_varextract. Variants were filtered using mimodd_vcf_filter so that only those that are present in one mutant strain but not in other mutant strains or the parent strain were kept. The filtered variants were then rebased to the ce11 assembly using mimodd_rebase and annotated with the SnpEff4.3 WBcel235.86 file. The annotated variants were finally exported using the MiModD Report Variants tool.

Usually, the variants in a certain mutant strain are enriched on one chromosome since backcrosses removed most unlinked variants. The mutations predicted to have the most severe effect on protein coding (stop gain, splicing mutations) on that chromosome were then further tested by fosmid rescue or mutants.

Imaging

Worms were immobilized with 10mM levamisole and mounted on a 3% agarose pad on a glass slide. To image the entire PVQ neuron including the nerve ring, we used a spinning disc confocal microscope (Nikon Ti-E Eclipse inverted scope equipped with 488 and 561 laser lines, a Prior NZ250 Piezo stage, a PerkinElmer UltraVIEW VoX, a Hamamatsu C9100-50 camera and a CFI Plan Fluor 40X oil objective (1.3 NA)). Volocity software (PerkinElmer) were used to acquire images and automatically

bioRxiv preprint doi: https://doi.org/10.1101/2021.09.12.459970; this version posted September 12, 2021. The copyright holder for this preprint (which was not certified by peer review) is the author/funder, who has granted bioRxiv a license to display the preprint in perpetuity. It is made available under aCC-BY-NC 4.0 International license.

stitch them. Images that only cover a part of PVQ (no stitching) were performed on a Leica DMi8 microscope equipped with a Visitech i-SIM super-resolution confocal system, 488, 561 and 637 laser lines, an ASI-XYpZ Piezo stage and a Hamamatsu ORCA-Flash4.0 CMOS camera. MetaMorph Imaging software (Molecular Devices) was used to acquire these images.

Imaging analysis was performed with ImageJ. Image z-stacks were first projected using maximum projection. To quantify mitochondria density, mitochondria puncta in axons were identified based on manual thresholding. Both the proximal axon region and the distal axon region in each worm were included. For endogenous protein labeling, GFP intensity was background-subtracted, measured, and normalized to the control. In the distal axon, we focused on the region before the axon joins the nerve ring and becomes undistinguishable from the head neurons. PVQ axons shown in figures are often straightened in ImageJ.

Time course images of PVQ degeneration from L4 to 1doa were acquired on the i-SIM microscope. Individual worms were first imaged at early L4 stage (0hr) as described above. Worms were then transferred to OP50 seeded plates and allowed to recover before they were imaged again. Each worm was imaged five times in total (0hr, 4hr, 8hr, 12hr and 24hr).

Laser axotomy

Laser axotomy was performed as described previously (Byrne et al., 2011). L4 animals were immobilized with M9 containing 0.05 μm diameter polystyrene beads (Polysciences) and mounted on a 3% agarose pad on a glass slide. Animals were visualized with a Nikon Eclipse 80i microscope using a 100x Plan Apo VC lens (1.4 NA). One of the two PVQ axons in each worm was cut at the vulval region with 10 pulses of a 435 nm Micropoint laser at 20 Hz. Animals were then recovered to OP50 seeded NGM plates and analyzed 24 hours later for axon degeneration.

Calsyntenins sequence alignment

Alignment of Calsyntenin protein sequences was performed in Jalview (Waterhouse et al., 2009) using the ClustalO algorithm with default settings.

bioRxiv preprint doi: https://doi.org/10.1101/2021.09.12.459970; this version posted September 12, 2021. The copyright holder for this preprint (which was not certified by peer review) is the author/funder, who has granted bioRxiv a license to display the preprint in perpetuity. It is made available under aCC-BY-NC 4.0 International license.

Quantification and statistical analysis

For axon degeneration analyses, fraction of worms with two intact (non-truncated) axons was quantified, and the data were expressed as proportion ± 95% confidence of interval. Two-sided Fisher's exact tests were performed on these binary data in GraphPad Prism. For non-binary data, multiple conditions were compared by Kruskal-Wallis nonparametric ANOVA test, followed by Dunn's multiple comparisons test. Other statistical tests were also described in the figure legends.

Materials Availability

Plasmids and strains utilized in this study will be made available to the scientific community upon request directed to Dr. Hammarlund. Strains generated in this study will be deposited at the Caenorhabditis Genetics Center (CGC).

bioRxiv preprint doi: https://doi.org/10.1101/2021.09.12.459970; this version posted September 12, 2021. The copyright holder for this preprint (which was not certified by peer review) is the author/funder, who has granted bioRxiv a license to display the preprint in perpetuity. It is made available under aCC-BY-NC 4.0 International license.

KEY RESOURCES TABLE

REAGENT or RESOURCE	SOURCE	IDENTIFIER
Chemicals, Peptides, and Recombinant Proteins		
Levamisole hydrochloride	Santa Cruz Biotechnology	Cat#sc-205730
Proteinase K	Sigma	Cat#3115879001
Polybead® Microspheres 0.05µm	Polysciences	Cat#08691
Gateway™ LR Clonase™ II Enzyme mix	Invitrogen	Cat#11791020
1kb DNA Ladder	Promega	Cat#G571A
Alt-R® S.p. Cas9 Nuclease V3	IDT	Cat#1081058
tracrRNA	IDT	Cat#1072532
Ethyl methanesulfonate	Sigma	Cat#M0880
QIAprep Spin Miniprep Kit	Qiagen	Cat#27106
Phusion® High-Fidelity DNA Polymerase	NEB	Cat#M0530L
Nonidet P-40	americanBIO	Cat#AB01425
TWEEN® 20	Sigma	Cat#P5927
Gelatin	MP Biomedicals	Cat#901771
β-Mercaptoethanol	Sigma	Cat#M3148-25ML
UltraPure™ Phenol:Chloroform:Isoamyl Alcohol	Invitrogen	Cat#15593031
Sodium Acetate, 3M solution, pH5.2	americanBIO	Cat#AB13168-01000
Nuclease free water	americanBIO	Cat#AB02123-00500
Experimental Models: Organisms/Strains		
C. elegans: oyIs14[sra-6p::GFP] V	CGC	XE2047
C. elegans: oyIs14[sra-6p::GFP], ric-7(n2657) V	This study	XE2046
C. elegans: oyIs14[sra-6p::GFP] V; wpEx369[sra-6p::mito::TagRFP + odr-1p::RFP]	This study	XE2263
C. elegans: oyIs14[sra-6p::GFP], ric-7(n2657) V; wpEx369[sra-6p::mito::TagRFP + odr-1p::RFP]	This study	XE2264

bioRxiv preprint doi: https://doi.org/10.1101/2021.09.12.459970; this version posted September 12, 2021. The copyright holder for this preprint (which was not certified by peer review) is the author/funder, who has granted bioRxiv a license to display the preprint in perpetuity. It is made available under aCC-BY-NC 4.0 International license.

C. elegans: oyIs14[sra-6p::GFP], ric-7(n2657) V; casy-1(wp60) II	This study	XE2209
C. elegans: oyIs14[sra-6p::GFP], ric-7(n2657) V; unc-43(wp64) II	This study	XE2210
C. elegans: ric-7(n2657) V; casy-1(wp78) II; wpEx370[sra-6p::casy-1c::GFP + sra-6p::TagRFP + odr-1p::RFP]	This study	XE2265
C. elegans: casy-1(wp78) II; wpEx370[sra-6p::casy-1c::GFP + sra-6p::TagRFP + odr-1p::RFP]	This study	XE2266
C. elegans: oyIs14[sra-6p::GFP], ric-7(n2657) V; unc-43(wp64) IV; wpEx369[sra-6p::mito::TagRFP + odr-1p::RFP]	This study	XE2618
C. elegans: oyIs14[sra-6p::GFP], ric-7(n2657) V; casy-1(wp60) II; wpEx371[sra-6p::mito::TagRFP + odr-1p::RFP]	This study	XE2269
C. elegans: oyIs14[sra-6p::GFP], ric-7(n2657) V; casy-1(wp60) II; wpEx374[sra-6p::casy-1a::SL2::mcherry + myo-2p::mcherry]	This study	XE2274
C. elegans: oyIs14[sra-6p::GFP], ric-7(n2657) V; casy-1(wp60) II; wpEx375[sra-6p::casy-1b::SL2::mcherry + myo-2p::mcherry]	This study	XE2275
C. elegans: oyIs14[sra-6p::GFP], ric-7(n2657) V; casy-1(wp60) II; wpEx376[sra-6p::casy-1c::SL2::mcherry + myo-2p::mcherry]	This study	XE2276
C. elegans: oyIs14[sra-6p::GFP], ric-7(n2657) V; casy-1(wp60) II; wpEx379[sra-6p::casy-1a no KBS::SL2::mcherry + myo-2p::mcherry]	This study	XE2277
C. elegans: oyIs14[sra::gfp], ric-7(n2657) V; casy-1(wp60) II; wpEx407[sra-6p::casy-1c_delta_extracellular::SL2::mCherry + myo-2p::mCherry];	This study	XE2355
C. elegans: oyIs14[sra-6p::GFP], ric-7(n2657) V; casy-1(wp60) II; wpEx380[sra-6p::casy-1 cytoplasmic domain::SL2::mcherry + myo-2p::mcherry]	This study	XE2278
C. elegans: oyIs14[sra-6p::GFP] V; casy-1(wp60) II	This study	XE2374

bioRxiv preprint doi: https://doi.org/10.1101/2021.09.12.459970; this version posted September 12, 2021. The copyright holder for this preprint (which was not certified by peer review) is the author/funder, who has granted bioRxiv a license to display the preprint in perpetuity. It is made available under aCC-BY-NC 4.0 International license.

C. elegans: oyIs14[sra-6p::GFP] V; casy-1(wp60) II; wpEx376[sra-6p::casy-1c::SL2::mcherry + myo-2p::mcherry]	This study	XE2544
C. elegans: oyIs14[sra-6p::GFP], ric-7(n2657) V; wpEx438[sra-6p::casy-1c mutated acidic region::SL2::mcherry + myo-2p::mcherry]	This study	XE2547
C. elegans: oyIs14[sra::gfp], ric-7(n2657) V; casy-1(wp60) II; wpEx431[sra-6p::casy-1(WW-AA)::SL2::mCherry + myo-2p::mCherry]	This study	XE2504
C. elegans: oyIs14[sra-6p::GFP], ric-7(n2657) V; wpEx381[sra-6p::unc-116::GFP::tomm-7 + sra-6p::mito::TagRFP + odr-1p::RFP]	This study	XE2279
C. elegans: oyIs14[sra-6p::GFP], ric-7(n2657), klc-2(km11) V	This study	XE2350
C. elegans: oyIs14[sra-6p::GFP], ric-7(n2657) V; klc-1(ok2609) IV	This study	XE2290
C. elegans: oyIs14[sra-6p::GFP], ric-7(n2657) V; tir-1(qd4) III	This study	XE2308
C. elegans: oyIs14[sra-6p::GFP], ric-7(n2657) V; tir-1(ok2859) III	This study	XE2309
C. elegans: oyIs14[sra-6p::GFP], ric-7(n2657) V; casy-1(tm718) II	This study	XE2294
C. elegans: oyIs14[sra-6p::GFP], ric-7(n2657) V; casy-1(wp78) II	This study	XE2262
C. elegans: casy-1(wp78) II	This study	XE2260
C. elegans: oyIs14[sra-6p::GFP], ric-7(n2657) V; casy-1(wp60); wpEx397[WRM0622dH03 + myo-2p::mCherry]	This study	XE2313
C. elegans: oyIs14[sra-6p::GFP], ric-7(n2657) V; unc-43(n498sd) IV	This study	XE2419
C. elegans: oyIs14[sra-6p::GFP], ric-7(n2657) V; unc-43(e408) IV	This study	XE2423
C. elegans: ric-7(n2657) V; casy-1(wp78) II	This study	XE2244
C. elegans: oyIs14[sra-6p::GFP], ric-7(n2657) V; lin-10(n1853) I	This study	XE2428

bioRxiv preprint doi: https://doi.org/10.1101/2021.09.12.459970; this version posted September 12, 2021. The copyright holder for this preprint (which was not certified by peer review) is the author/funder, who has granted bioRxiv a license to display the preprint in perpetuity. It is made available under aCC-BY-NC 4.0 International license.

C. elegans: oyIs14[sra-6p::GFP], ric-7(n2657) V; unc-43(e408) IV; casy-1(wp78) II	This study	XE2429
C. elegans: wpIs141[sra-6p::GFP1-10 + myo-2p::mcherry]	This study	XE2441
C. elegans: oyIs14[sra-6p::GFP], ric-7(n2657) V; lin-10(n1853) I; unc-43(e408) IV	This study	XE2508
C. elegans: oyIs14[sra-6p::GFP], ric-7(n2657) V; lin-10(e1439) I	This study	XE2490
C. elegans: oyIs14[sra-6p::GFP] V; unc-43(e408) IV	This study	XE2580
C. elegans: oyIs14[sra-6p::GFP], ric-7(n2657) V; unc-43(e408) IV; casy-1(wp78) II + wpEx430[sra-6p::unc-43g + myo-2p::mcherry]	This study	XE2496
C. elegans: oyIs14[sra-6p::GFP], ric-7(n2657) V; unc-43(e408) IV; casy-1(wp78) II + wpEx432[sra-6p::unc-43g T284D::SL2::mcherry + myo-2p::mcherry]	This study	XE2506
C. elegans: oyIs14[sra-6p::GFP], ric-7(n2657) V; lin-10(e1439) I; unc-43(e408) IV	This study	XE2530
C. elegans: oyIs14[sra-6p::GFP], ric-7(n2657) V; unc-2(e55) X; casy-1(wp78) II	This study	XE2546
C. elegans: ric-7(n2657) V; unc-43(wp106[unc-43::gfp11x7]) IV; wpIs141[sra-6p::GFP1-10 + myo-2p::mcherry] II	This study	XE2564
C. elegans: ric-7(n2657) V; unc-43(wp106[unc-43::gfp11x7]) IV; wpIs141[sra-6p::GFP1-10 + myo-2p::mcherry], casy-1(wp78) II	This study	XE2565
C. elegans: unc-43(wp106[unc-43::gfp11x7]) IV; wpIs141[sra-6p::GFP1-10 + myo-2p::mcherry] II	This study	XE2567
C. elegans: ric-7(n2657) V; lin-10(e1439) I; unc-43(wp106[unc-43::gfp11x7]) IV; wpIs141[sra-6p::GFP1-10 + myo-2p::mcherry] II	This study	XE2605
C. elegans: ric-7(n2657) V; unc-43(wp106[unc-43::gfp11x7]) IV; wpIs141[sra-6p::GFP1-10 + myo-2p::mcherry] II; wpEx450[sra-6p::unc-116::tomm-7 + odr-1p::RFP]	This study	XE2649
C. elegans: casy-1(syb3311[casy-1::gfp11x7]) II	This study	PHX3311

bioRxiv preprint doi: https://doi.org/10.1101/2021.09.12.459970; this version posted September 12, 2021. The copyright holder for this preprint (which was not certified by peer review) is the author/funder, who has granted bioRxiv a license to display the preprint in perpetuity. It is made available under aCC-BY-NC 4.0 International license.

C. elegans: oyIs14[sra-6p::GFP], ric-7(n2657), klc-2(km11) V; unc-43(e408)	This study	XE2575
C. elegans: casy-1(syb3311[casy-1::gfp11x7]), wpIs141[sra-6p::GFP1-10 + myo-2p::mcherry] II	This study	XE2593
C. elegans: casy-1(syb3311[casy-1::gfp11x7]), wpIs141[sra-6p::GFP1-10 + myo-2p::mcherry] II; ric-7(n2657) V	This study	XE2594
C. elegans: casy-1(syb3311[casy-1::gfp11x7]), wpIs141[sra-6p::GFP1-10 + myo-2p::mcherry] II; klc-2(km11) V	This study	XE2595
C. elegans: oyIs14[sra-6p::GFP], ric-7(n2657) V; unc-2(e55) X; lin-10(n1853) I	This study	XE2585
C. elegans: lin-10(wp109[lin-10::gfp11x7]) I; wpIs141[sra-6p::GFP1-10 + myo-2p::mcherry] II	This study	XE2586
C. elegans: lin-10(wp109[lin-10::gfp11x7]) I; wpIs141[sra-6p::GFP1-10 + myo-2p::mcherry] casy-1(wp78) II	This study	XE2587
C. elegans: oyIs14[sra-6p::GFP], ric-7(n2657) V; egl-19(n582) IV; casy-1(wp78) II	This study	XE2606
C. elegans: oyIs14[sra-6p::GFP], ric-7(n2657) V; egl-19(n582) IV; lin-10(n1853) I	This study	XE2607
C. elegans: oyIs14[sra-6p::GFP], ric-7(n2657) V; unc-36(e251) III; casy-1(wp78) II	This study	XE2608
C. elegans: oyIs14[sra-6p::GFP], ric-7(n2657) V; unc-36(e251) III; lin-10(n1853) I	This study	XE2609
C. elegans: oyIs14[sra-6p::GFP], ric-7(n2657) V; casy-1(syb3311[casy-1::gfp11x7]) II	This study	XE2610
C. elegans: oyIs14[sra-6p::GFP], ric-7(n2657) V; apl-1(wp19) X	This study	XE2415
C. elegans: oyIs14[sra-6p::GFP], ric-7(n2657) V; apl-1(wp19) X; wpIs146[sra-6p::nCre + odr-1p::RFP]	This study	XE2634
C. elegans: oyIs14[sra-6p::GFP], ric-7(n2657) V; wpIs146[sra-6p::nCre + odr-1p::RFP]	This study	XE2698
C. elegans: oyIs14[sra-6p::GFP], ric-7(n2657) V; apl-1(wp22) X	This study	XE2489

bioRxiv preprint doi: https://doi.org/10.1101/2021.09.12.459970; this version posted September 12, 2021. The copyright holder for this preprint (which was not certified by peer review) is the author/funder, who has granted bioRxiv a license to display the preprint in perpetuity. It is made available under aCC-BY-NC 4.0 International license.

C. elegans: oyIs14[sra-6p::GFP] V; egl-19(n582) IV	This study	XE2640
C. elegans: oyIs14[sra-6p::GFP] V; unc-36(e251) III	This study	XE2641
C. elegans: oyIs14[sra-6p::GFP], ric-7(n2657) V; unc-43(n498sd) IV; unc-36(e251) III	This study	XE2648
C. elegans: oyIs14[sra-6p::GFP], ric-7(n2657) V; unc-43(n498sd) IV; tir-1(qd4) III	This study	XE2652
C. elegans: oyIs14[sra-6p::GFP], ric-7(n2657) V; unc-43(n498sd) IV; nsy-1(ok593) II	This study	XE2653
C. elegans: oyIs14[sra-6p::GFP], ric-7(n2657) V; unc-43(n498sd), pmk1(km25) IV	This study	XE2655
C. elegans: oyIs14[sra-6p::GFP], ric-7(n2657) V; casy-1(wp78) II; tir-1(qd4) III	This study	XE2656
C. elegans: oyIs14[sra-6p::GFP], ric-7(n2657) V; casy-1(wp78), nsy-1(ok593) II	This study	XE2657
C. elegans: oyIs14[sra-6p::GFP], ric-7(n2657) V; casy-1(wp78) II; sek-1(km4) X	This study	XE2658
C. elegans: oyIs14[sra-6p::GFP], ric-7(n2657) V; casy-1(wp78) II; pmk-1(km25) IV	This study	XE2659
C. elegans: oyIs14[sra-6p::GFP], ric-7(n2657) V; wpEx453[sra-6p::unc-43g T284D::SL2::mcherry + myo-2p::mcherry]	This study	XE2661
C. elegans: oyIs14[sra-6p::GFP], ric-7(n2657) V; wpEx452[sra-6p::unc-43g + myo-2p::mcherry]	This study	XE2662
C. elegans: oyIs14[sra-6p::GFP] V; unc-116(rh24sb79) III	This study	XE2411
C. elegans: oyIs14[sra-6p::GFP] V; unc-116(rh24sb79) III; unc-43(n498sd) IV	This study	XE2717
C. elegans: ric-7(n2657) V; unc-43(wp106[unc-43::gfp11X7]) IV; wpEx475[sra-6p::unc-116::GFP1-10 + myo-2p::mCherry]	This study	XE2752
C. elegans: oyIs14[sra-6p::GFP], ric-7(n2657) V; unc-43(wp106[unc-43::gfp11X7]) IV; wpEx475[sra-6p::unc-116::GFP1-10 + myo-2p::mCherry]	This study	XE2753
C. elegans: oyIs14[sra-6p::GFP] V; miro-1(wy50266) IV; mtx-2(wy50180) III	This study	XE2839

bioRxiv preprint doi: https://doi.org/10.1101/2021.09.12.459970; this version posted September 12, 2021. The copyright holder for this preprint (which was not certified by peer review) is the author/funder, who has granted bioRxiv a license to display the preprint in perpetuity. It is made available under aCC-BY-NC 4.0 International license.

C. elegans: oyIs14[sra-6p::GFP] V; trak-1(gk571211) I	This study	XE2840
C. elegans: oyIs14[sra-6p::GFP] V; miro-1(tm1966) IV; miro-2(tm2933) X	This study	XE2349
Oligonucleotides		
crRNA and genotyping primers for CRISPR experiments	This study	Table S1
Recombinant DNA		
Plasmid: sra-6p::casy-1a CDS::SL2::mCherry	This study	pCD1
Plasmid: sra-6p::casy-1b CDS::SL2::mCherry	This study	pCD2
Plasmid: sra-6p::casy-1c CDS::SL2::mCherry	This study	pCD3
Plasmid: sra-6p::casy-1a no KBS CDS::SL2::mCherry	This study	pCD4
Plasmid: sra-6p::casy-1 cytoplasmic CDS::SL2::mCherry	This study	pCD5
Plasmid: sra-6p::casy-1 CDS no ECD::SL2::mCherry	This study	pYW135
Plasmid: sra-6p::mito::tagRFP	This study	pCD6
Plasmid: sra-6p::unc-116::gfp::tomm7	This study	pCD7
Plasmid: sra-6p::unc-43g WT	This study	pCD8
Plasmid: sra-6p::unc-43g T286D::SL2::mCherry	This study	pCD9
Plasmid: sra-6p::GFP1-10	This study	pCD10
Plasmid: sra-6p::unc-116::tomm-7	This study	pCD11
Plasmid: sra-6p::casy-1c CDS-WWAA::SL2::mCherry	This study	pCD12
Plasmid: sra-6p::casy-1c CDS::mutated acidic region::SL2::mCherry	This study	pYW184
Plasmid: sra-6p::casy-1c::GFP	This study	pYW86
Plasmid: sra-6p::Cre	This study	pCD13
Plasmid: pRF4::rol-6(su1006)	Mello et al., 1991	pRF4
Plasmid: sra-6p::wt tir-1a::SL2::mCherry	This study	pCD14
Plasmid: sra-6p::unc-116::gfp1-10	This study	pCD15

bioRxiv preprint doi: https://doi.org/10.1101/2021.09.12.459970; this version posted September 12, 2021. The copyright holder for this preprint (which was not certified by peer review) is the author/funder, who has granted bioRxiv a license to display the preprint in perpetuity. It is made available under aCC-BY-NC 4.0 International license.

Software and Algorithms		
Fiji 1.53c	NIH	https://imagej.nih.gov/ij/download.html
MetaMorph, Version 7.10.2.240	Molecular Devices	https://mdc.custhelp.com/app/products/detail/p/13
Prism, Version 8	GraphPad	https://www.graphpad.com/scientific-software/prism/
Galaxy	Afgan et al., 2016	https://usegalaxy.org/
MiModD	Maier and Baumeiste, 2016	http://mimodd.readthedocs.io/en/latest/index.html
Bowtie2-2.3.4.2	Langmead and Salzberg, 2012	http://bowtie-bio.sourceforge.net/bowtie2/index.shtml
ApE	M. Wayne Davis	https://jorgensen.biology.utah.edu/wayned/ape/
Jalview, Version 2.11.1.2	Waterhouse et al., 2009	http://www.jalview.org/getdown/release/

bioRxiv preprint doi: https://doi.org/10.1101/2021.09.12.459970; this version posted September 12, 2021. The copyright holder for this preprint (which was not certified by peer review) is the author/funder, who has granted bioRxiv a license to display the preprint in perpetuity. It is made available under aCC-BY-NC 4.0 International license.

Acknowledgments

We thank Daniel Colon-Ramos's lab for sharing fosmids. We thank Shaul Yogev's lab for sharing strains, discussion of the project and guidance on whole-genome sequencing. We thank the Yale Center for Genome Analysis for performing the whole-genome sequencing. We thank the Cellular Neuroscience, Neurodegeneration and Repair (CNNR) imaging core for microscopy. We thank the international Caenorhabditis Genetics Center for strains. We are grateful to members of the Hammarlund lab for valuable comments. This work is supported by NIH grants R01 NS098817 and R01 NS094219 (to M.H.).

Author Contributions

C.D. and M.H. conceived the project. C.D. conducted and analyzed most experiments, wrote the original draft, and edited the final version. Y.W. generated the *unc-43::gfp11x7* and the *lin-10::gfp11x7* KI strains, helped with the *casy-1* rescue experiments, performed multiple injections and degeneration analyses, and helped edit final version of the draft. H.T. measured mitochondria density in axons, and helped edit final version of the draft. M.H. supervised the project, and edited the final version of the draft.

Competing Interests

The authors declare no competing interests.

bioRxiv preprint doi: https://doi.org/10.1101/2021.09.12.459970; this version posted September 12, 2021. The copyright holder for this preprint (which was not certified by peer review) is the author/funder, who has granted bioRxiv a license to display the preprint in perpetuity. It is made available under aCC-BY-NC 4.0 International license.

References

Abiria, S.A., and Colbran, R.J. (2010). CaMKII associates with CaV1.2 L-type calcium channels via selected beta subunits to enhance regulatory phosphorylation. J Neurochem *112*, 150-161.

Afgan, E., Baker, D., van den Beek, M., Blankenberg, D., Bouvier, D., Cech, M., Chilton, J., Clements, D., Coraor, N., Eberhard, C.*, et al.* (2016). The Galaxy platform for accessible, reproducible and collaborative biomedical analyses: 2016 update. Nucleic Acids Res *44*, W3-W10.

Alavi, M.V., and Fuhrmann, N. (2013). Dominant optic atrophy, OPA1, and mitochondrial quality control: understanding mitochondrial network dynamics. Mol Neurodegener *8*, 32.

Alloway, P.G., Howard, L., and Dolph, P.J. (2000). The formation of stable rhodopsin-arrestin complexes induces apoptosis and photoreceptor cell degeneration. Neuron *28*, 129-138.

Alqadah, A., Hsieh, Y.W., Schumacher, J.A., Wang, X., Merrill, S.A., Millington, G., Bayne, B., Jorgensen, E.M., and Chuang, C.F. (2016a). SLO BK Potassium Channels Couple Gap Junctions to Inhibition of Calcium Signaling in Olfactory Neuron Diversification. PLoS Genet *12*, e1005654.

Alqadah, A., Hsieh, Y.W., Xiong, R., and Chuang, C.F. (2016b). Stochastic left-right neuronal asymmetry in Caenorhabditis elegans. Philos Trans R Soc Lond B Biol Sci *371*.

Alther, T.A., Domanitskaya, E., and Stoeckli, E.T. (2016). Calsyntenin 1-mediated trafficking of axon guidance receptors regulates the switch in axonal responsiveness at a choice point. Development *143*, 994-1004.

Araki, Y., Kawano, T., Taru, H., Saito, Y., Wada, S., Miyamoto, K., Kobayashi, H., Ishikawa, H.O., Ohsugi, Y., Yamamoto, T.*, et al.* (2007). The novel cargo Alcadein induces vesicle association of kinesin-1 motor components and activates axonal transport. EMBO J *26*, 1475-1486.

Araki, Y., Miyagi, N., Kato, N., Yoshida, T., Wada, S., Nishimura, M., Komano, H., Yamamoto, T., De Strooper, B., Yamamoto, K.*, et al.* (2004). Coordinated metabolism of Alcadein and amyloid beta-protein precursor regulates FE65-dependent gene transactivation. J Biol Chem *279*, 24343-24354.

Araki, Y., Tomita, S., Yamaguchi, H., Miyagi, N., Sumioka, A., Kirino, Y., and Suzuki, T. (2003). Novel cadherin-related membrane proteins, Alcadeins, enhance the X11-like protein-mediated stabilization of amyloid beta-protein precursor metabolism. J Biol Chem *278*, 49448-49458.

Bezprozvanny, I. (2009). Calcium signaling and neurodegenerative diseases. Trends Mol Med *15*, 89-100.

Blackstone, C. (2018). Converging cellular themes for the hereditary spastic paraplegias. Curr Opin Neurobiol *51*, 139-146.

Byrne, A.B., Edwards, T.J., and Hammarlund, M. (2011). In vivo Laser Axotomy in C. elegans. Journal of Visualized Experiments : JoVE, 2707.

Camins, A., Verdaguer, E., Folch, J., and Pallas, M. (2006). Involvement of calpain activation in neurodegenerative processes. CNS Drug Rev *12*, 135-148.

Catterall, W.A. (2011). Voltage-gated calcium channels. Cold Spring Harb Perspect Biol *3*, a003947.

Caylor, R.C., Jin, Y., and Ackley, B.D. (2013). The Caenorhabditis elegans voltage-gated calcium channel subunits UNC-2 and UNC-36 and the calcium-dependent kinase UNC-43/CaMKII regulate neuromuscular junction morphology. Neural Dev *8*, 10.

Chuang, C.F., and Bargmann, C.I. (2005). A Toll-interleukin 1 repeat protein at the synapse specifies asymmetric odorant receptor expression via ASK1 MAPKKK signaling. Genes Dev *19*, 270-281.

Ding, C., and Hammarlund, M. (2018). Aberrant information transfer interferes with functional axon regeneration. eLife *7*, e38829.

Essuman, K., Summers, D.W., Sasaki, Y., Mao, X., DiAntonio, A., and Milbrandt, J. (2017). The SARM1 Toll/Interleukin-1 Receptor Domain Possesses Intrinsic NAD^+ Cleavage Activity that Promotes Pathological Axonal Degeneration. Neuron *93*, 1334-1343 e1335.

bioRxiv preprint doi: https://doi.org/10.1101/2021.09.12.459970; this version posted September 12, 2021. The copyright holder for this preprint (which was not certified by peer review) is the author/funder, who has granted bioRxiv a license to display the preprint in perpetuity. It is made available under aCC-BY-NC 4.0 International license.

Frokjaer-Jensen, C., Kindt, K.S., Kerr, R.A., Suzuki, H., Melnik-Martinez, K., Gerstbreih, B., Driscol, M., and Schafer, W.R. (2006). Effects of voltage-gated calcium channel subunit genes on calcium influx in cultured C. elegans mechanosensory neurons. J Neurobiol *66*, 1125-1139.

Gerdts, J., Brace, E.J., Sasaki, Y., DiAntonio, A., and Milbrandt, J. (2015). SARM1 activation triggers axon degeneration locally via NAD^+ destruction. Science *348*, 453.

Gerdts, J., Summers, D.W., Sasaki, Y., DiAntonio, A., and Milbrandt, J. (2013). Sarm1-Mediated Axon Degeneration Requires Both SAM and TIR Interactions. The Journal of Neuroscience *33*, 13569.

Ghanta, K.S., and Mello, C.C. (2020). Melting dsDNA Donor Molecules Greatly Improves Precision Genome Editing in Caenorhabditis elegans. Genetics.

Ghose, P., Park, E.C., Tabakin, A., Salazar-Vasquez, N., and Rongo, C. (2013). Anoxia-reoxygenation regulates mitochondrial dynamics through the hypoxia response pathway, SKN-1/Nrf, and stomatin-like protein STL-1/SLP-2. PLoS Genet *9*, e1004063.

Gibson, D.G., Young, L., Chuang, R.Y., Venter, J.C., Hutchison, C.A., 3rd, and Smith, H.O. (2009). Enzymatic assembly of DNA molecules up to several hundred kilobases. Nat Methods *6*, 343-345.

Glater, E.E., Megeath, L.J., Stowers, R.S., and Schwarz, T.L. (2006). Axonal transport of mitochondria requires milton to recruit kinesin heavy chain and is light chain independent. J Cell Biol *173*, 545-557.

Gotoh, N., Saito, Y., Hata, S., Saito, H., Ojima, D., Murayama, C., Shigeta, M., Abe, T., Konno, D., Matsuzaki, F.*, et al.* (2020). Amyloidogenic processing of amyloid beta protein precursor (APP) is enhanced in the brains of alcadein alpha-deficient mice. J Biol Chem *295*, 9650-9662.

Grunewald, A., Kumar, K.R., and Sue, C.M. (2019). New insights into the complex role of mitochondria in Parkinson's disease. Prog Neurobiol *177*, 73-93.

Guedes-Dias, P., and Holzbaur, E.L.F. (2019). Axonal transport: Driving synaptic function. Science *366*.

Guo, X., Macleod, G.T., Wellington, A., Hu, F., Panchumarthi, S., Schoenfield, M., Marin, L., Charlton, M.P., Atwood, H.L., and Zinsmaier, K.E. (2005). The GTPase dMiro is required for axonal transport of mitochondria to Drosophila synapses. Neuron *47*, 379-393.

Guo, X., Zhou, J., Starr, C., Mohns, E.J., Li, Y., Chen, E.P., Yoon, Y., Kellner, C.P., Tanaka, K., Wang, H.*, et al.* (2021). Preservation of vision after CaMKII-mediated protection of retinal ganglion cells. Cell *184*, 4299-4314 e4212.

Halestrap, A.P. (2009). What is the mitochondrial permeability transition pore? J Mol Cell Cardiol *46*, 821-831.

Halt, A.R., Dallapiazza, R.F., Zhou, Y., Stein, I.S., Qian, H., Juntti, S., Wojcik, S., Brose, N., Silva, A.J., and Hell, J.W. (2012). CaMKII binding to GluN2B is critical during memory consolidation. EMBO J *31*, 1203-1216.

Hata, S., Fujishige, S., Araki, Y., Kato, N., Araseki, M., Nishimura, M., Hartmann, D., Saftig, P., Fahrenholz, F., Taniguchi, M.*, et al.* (2009). Alcadein cleavages by amyloid beta-precursor protein (APP) alpha- and gamma-secretases generate small peptides, p3-Alcs, indicating Alzheimer disease-related gamma-secretase dysfunction. J Biol Chem *284*, 36024-36033.

Hauptmann, S., Keil, U., Scherping, I., Bonert, A., Eckert, A., and Muller, W.E. (2006). Mitochondrial dysfunction in sporadic and genetic Alzheimer's disease. Exp Gerontol *41*, 668-673.

Hayakawa, T., Matsuzawa, A., Noguchi, T., Takeda, K., and Ichijo, H. (2006). The ASK1-MAP kinase pathways in immune and stress responses. Microbes Infect *8*, 1098-1107.

He, S., Cuentas-Condori, A., and Miller, D.M., 3rd (2019). NATF (Native and Tissue-Specific Fluorescence): A Strategy for Bright, Tissue-Specific GFP Labeling of Native Proteins in Caenorhabditis elegans. Genetics *212*, 387-395.

Hell, J.W. (2014). CaMKII: claiming center stage in postsynaptic function and organization. Neuron *81*, 249-265.

bioRxiv preprint doi: https://doi.org/10.1101/2021.09.12.459970; this version posted September 12, 2021. The copyright holder for this preprint (which was not certified by peer review) is the author/funder, who has granted bioRxiv a license to display the preprint in perpetuity. It is made available under aCC-BY-NC 4.0 International license.

Hell, J.W., Westenbroek, R.E., Breeze, L.J., Wang, K.K., Chavkin, C., and Catterall, W.A. (1996). N-methyl-D-aspartate receptor-induced proteolytic conversion of postsynaptic class C L-type calcium channels in hippocampal neurons. Proc Natl Acad Sci U S A *93*, 3362-3367.

Henninger, N., Bouley, J., Sikoglu, E.M., An, J., Moore, C.M., King, J.A., Bowser, R., Freeman, M.R., and Brown, R.H., Jr. (2016). Attenuated traumatic axonal injury and improved functional outcome after traumatic brain injury in mice lacking Sarm1. Brain *139*, 1094-1105.

Hill, E., Broadbent, I.D., Chothia, C., and Pettitt, J. (2001). Cadherin superfamily proteins in Caenorhabditis elegans and Drosophila melanogaster. J Mol Biol *305*, 1011-1024.

Hobert, O. (2013). The neuronal genome of Caenorhabditis elegans. WormBook, 1-106.

Hollenbeck, P.J., and Saxton, W.M. (2005). The axonal transport of mitochondria. J Cell Sci *118*, 5411-5419.

Hoppe, U.C. (2010). Mitochondrial calcium channels. FEBS Lett *584*, 1975-1981.

Hou, S.T., Jiang, S.X., Aylsworth, A., Ferguson, G., Slinn, J., Hu, H., Leung, T., Kappler, J., and Kaibuchi, K. (2009). CaMKII phosphorylates collapsin response mediator protein 2 and modulates axonal damage during glutamate excitotoxicity. J Neurochem *111*, 870-881.

Hsu, J.M., Kang, Y., Corty, M.M., Mathieson, D., Peters, O.M., and Freeman, M.R. (2020). Injury-Induced Inhibition of Bystander Neurons Requires dSarm and Signaling from Glia. Neuron.

Hudmon, A., Schulman, H., Kim, J., Maltez, J.M., Tsien, R.W., and Pitt, G.S. (2005). CaMKII tethers to L-type Ca2+ channels, establishing a local and dedicated integrator of Ca2+ signals for facilitation. J Cell Biol *171*, 537-547.

Jaussi, R., Cotton, B., Juretic, N., Christen, P., and Schumperli, D. (1985). The primary structure of the precursor of chicken mitochondrial aspartate aminotransferase. Cloning and sequence analysis of cDNA. J Biol Chem *260*, 16060-16063.

Kim, D.H., Feinbaum, R., Alloing, G., Emerson, F.E., Garsin, D.A., Inoue, H., Tanaka-Hino, M., Hisamoto, N., Matsumoto, K., Tan, M.W*., et al.* (2002). A conserved p38 MAP kinase pathway in Caenorhabditis elegans innate immunity. Science *297*, 623-626.

Kim, H., Kim, D., Kim, J., Lee, H.-Y., Park, D., Kang, H., Matsuda, K., Sterky, F.H., Yuzaki, M., Kim, J.Y*., et al.* (2020a). Calsyntenin-3 directly interacts with neurexins to orchestrate excitatory synapse development in the hippocampus. bioRxiv, 2020.2001.2024.918722.

Kim, H., Kim, D., Kim, J., Lee, H.Y., Park, D., Kang, H., Matsuda, K., Sterky, F.H., Yuzaki, M., Kim, J.Y*., et al.* (2020b). Calsyntenin-3 interacts with both alpha- and beta-neurexins in the regulation of excitatory synaptic innervation in specific Schaffer collateral pathways. J Biol Chem *295*, 9244-9262.

Konecna, A., Frischknecht, R., Kinter, J., Ludwig, A., Steuble, M., Meskenaite, V., Indermuhle, M., Engel, M., Cen, C., Mateos, J.M*., et al.* (2006). Calsyntenin-1 docks vesicular cargo to kinesin-1. Mol Biol Cell *17*, 3651-3663.

Kristaponyte, I., Hong, Y., Lu, H., and Shieh, B.H. (2012). Role of rhodopsin and arrestin phosphorylation in retinal degeneration of Drosophila. J Neurosci *32*, 10758-10766.

Langmead, B., and Salzberg, S.L. (2012). Fast gapped-read alignment with Bowtie 2. Nat Methods *9*, 357-359.

Lee, T.J., Lee, J.W., Haynes, E.M., Eliceiri, K.W., and Halloran, M.C. (2017). The Kinesin Adaptor Calsyntenin-1 Organizes Microtubule Polarity and Regulates Dynamics during Sensory Axon Arbor Development. Front Cell Neurosci *11*, 107.

Lipina, T.V., Prasad, T., Yokomaku, D., Luo, L., Connor, S.A., Kawabe, H., Wang, Y.T., Brose, N., Roder, J.C., and Craig, A.M. (2016). Cognitive Deficits in Calsyntenin-2-deficient Mice Associated with Reduced GABAergic Transmission. Neuropsychopharmacology *41*, 802-810.

Lisman, J., Schulman, H., and Cline, H. (2002). The molecular basis of CaMKII function in synaptic and behavioural memory. Nat Rev Neurosci *3*, 175-190.

bioRxiv preprint doi: https://doi.org/10.1101/2021.09.12.459970; this version posted September 12, 2021. The copyright holder for this preprint (which was not certified by peer review) is the author/funder, who has granted bioRxiv a license to display the preprint in perpetuity. It is made available under aCC-BY-NC 4.0 International license.

908 Loreto, A., Hill, C.S., Hewitt, V.L., Orsomando, G., Angeletti, C., Gilley, J., Lucci, C., Sanchez-Martinez, A.,
909 Whitworth, A.J., Conforti, L.*, et al.* (2020). Mitochondrial impairment activates the Wallerian pathway
910 through depletion of NMNAT2 leading to SARM1-dependent axon degeneration. Neurobiol Dis *134*,
911 104678.
912 Ludwig, A., Blume, J., Diep, T.M., Yuan, J., Mateos, J.M., Leuthauser, K., Steuble, M., Streit, P., and
913 Sonderegger, P. (2009). Calsyntenins mediate TGN exit of APP in a kinesin-1-dependent manner. Traffic
914 *10*, 572-589.
915 Maier, W., and Baumeiste, R. (2016). Mutation identification in model organism genomes using desktop
916 PCs. https://celegansde/mimodd/.
917 Marambaud, P., Dreses-Werringloer, U., and Vingtdeux, V. (2009). Calcium signaling in
918 neurodegeneration. Mol Neurodegener *4*, 20.
919 Maximov, A., and Bezprozvanny, I. (2002). Synaptic targeting of N-type calcium channels in hippocampal
920 neurons. J Neurosci *22*, 6939-6952.
921 Maximov, A., Südhof, T.C., and Bezprozvanny, I. (1999). Association of Neuronal Calcium Channels with
922 Modular Adaptor Proteins. Journal of Biological Chemistry *274*, 24453-24456.
923 Mello, C.C., Kramer, J.M., Stinchcomb, D., and Ambros, V. (1991). Efficient gene transfer in C.elegans:
924 extrachromosomal maintenance and integration of transforming sequences. EMBO J *10*, 3959-3970.
925 Merrill, M.A., Chen, Y., Strack, S., and Hell, J.W. (2005). Activity-driven postsynaptic translocation of
926 CaMKII. Trends Pharmacol Sci *26*, 645-653.
927 Neukomm, L.J., Burdett, T.C., Seeds, A.M., Hampel, S., Coutinho-Budd, J.C., Farley, J.E., Wong, J.,
928 Karadeniz, Y.B., Osterloh, J.M., Sheehan, A.E.*, et al.* (2017). Axon Death Pathways Converge on
929 Axundead to Promote Functional and Structural Axon Disassembly. Neuron *95*, 78-91 e75.
930 Nichols, A.L.A., Meelkop, E., Linton, C., Giordano-Santini, R., Sullivan, R.K., Donato, A., Nolan, C., Hall,
931 D.H., Xue, D., Neumann, B.*, et al.* (2016). The Apoptotic Engulfment Machinery Regulates Axonal
932 Degeneration in C. elegans Neurons. Cell Rep *14*, 1673-1683.
933 Nolan, K.M., Sarafi-Reinach, T.R., Horne, J.G., Saffer, A.M., and Sengupta, P. (2002). The DAF-7 TGF-beta
934 signaling pathway regulates chemosensory receptor gene expression in C. elegans. Genes Dev *16*, 3061-
935 3073.
936 Ohno, H., Kato, S., Naito, Y., Kunitomo, H., Tomioka, M., and Iino, Y. (2014). Role of synaptic
937 phosphatidylinositol 3-kinase in a behavioral learning response in C. elegans. Science *345*, 313-317.
938 Osterloh, J.M., Yang, J., Rooney, T.M., Fox, A.N., Adalbert, R., Powell, E.H., Sheehan, A.E., Avery, M.A.,
939 Hackett, R., Logan, M.A.*, et al.* (2012). dSarm/Sarm1 Is Required for Activation of an Injury-Induced Axon
940 Death Pathway. Science *337*, 481.
941 Otmakhov, N., Tao-Cheng, J.H., Carpenter, S., Asrican, B., Dosemeci, A., Reese, T.S., and Lisman, J.
942 (2004). Persistent accumulation of calcium/calmodulin-dependent protein kinase II in dendritic spines
943 after induction of NMDA receptor-dependent chemical long-term potentiation. J Neurosci *24*, 9324-
944 9331.
945 Pagano, D.J., Kingston, E.R., and Kim, D.H. (2015). Tissue expression pattern of PMK-2 p38 MAPK is
946 established by the miR-58 family in C. elegans. PLoS Genet *11*, e1004997.
947 Panneerselvam, P., Singh, L.P., Ho, B., Chen, J., and Ding, J.L. (2012). Targeting of pro-apoptotic TLR
948 adaptor SARM to mitochondria: definition of the critical region and residues in the signal sequence.
949 Biochem J *442*, 263-271.
950 Peters, O.M., Lewis, E.A., Osterloh, J.M., Weiss, A., Salameh, J.S., Metterville, J., Brown, R.H., and
951 Freeman, M.R. (2018). Loss of Sarm1 does not suppress motor neuron degeneration in the SOD1G93A
952 mouse model of amyotrophic lateral sclerosis. Hum Mol Genet.
953 Pettem, K.L., Yokomaku, D., Luo, L., Linhoff, M.W., Prasad, T., Connor, S.A., Siddiqui, T.J., Kawabe, H.,
954 Chen, F., Zhang, L.*, et al.* (2013). The specific alpha-neurexin interactor calsyntenin-3 promotes
955 excitatory and inhibitory synapse development. Neuron *80*, 113-128.

bioRxiv preprint doi: https://doi.org/10.1101/2021.09.12.459970; this version posted September 12, 2021. The copyright holder for this preprint (which was not certified by peer review) is the author/funder, who has granted bioRxiv a license to display the preprint in perpetuity. It is made available under aCC-BY-NC 4.0 International license.

Pickrell, A.M., and Youle, R.J. (2015). The roles of PINK1, parkin, and mitochondrial fidelity in Parkinson's disease. Neuron *85*, 257-273.

Ponomareva, O.Y., Holmen, I.C., Sperry, A.J., Eliceiri, K.W., and Halloran, M.C. (2014). Calsyntenin-1 regulates axon branching and endosomal trafficking during sensory neuron development in vivo. J Neurosci *34*, 9235-9248.

Preuschhof, C., Heekeren, H.R., Li, S.C., Sander, T., Lindenberger, U., and Backman, L. (2010). KIBRA and CLSTN2 polymorphisms exert interactive effects on human episodic memory. Neuropsychologia *48*, 402-408.

Rawson, R.L., Yam, L., Weimer, R.M., Bend, E.G., Hartwieg, E., Horvitz, H.R., Clark, S.G., and Jorgensen, E.M. (2014). Axons degenerate in the absence of mitochondria in C. elegans. Curr Biol *24*, 760-765.

Reiner, D.J., Newton, E.M., Tian, H., and Thomas, J.H. (1999). Diverse behavioural defects caused by mutations in Caenorhabditis elegans unc-43 CaM kinase II. Nature *402*, 199-203.

Rose, J., Jin, S.X., and Craig, A.M. (2009). Heterosynaptic molecular dynamics: locally induced propagating synaptic accumulation of CaM kinase II. Neuron *61*, 351-358.

Sagasti, A., Hisamoto, N., Hyodo, J., Tanaka-Hino, M., Matsumoto, K., and Bargmann, C.I. (2001). The CaMKII UNC-43 Activates the MAPKKK NSY-1 to Execute a Lateral Signaling Decision Required for Asymmetric Olfactory Neuron Fates. Cell *105*, 221-232.

Sakamoto, R., Byrd, D.T., Brown, H.M., Hisamoto, N., Matsumoto, K., and Jin, Y. (2005). The Caenorhabditis elegans UNC-14 RUN Domain Protein Binds to the Kinesin-1 and UNC-16 Complex and Regulates Synaptic Vesicle Localization. Molecular Biology of the Cell *16*, 483-496.

Schwarz, T.L. (2013). Mitochondrial trafficking in neurons. Cold Spring Harb Perspect Biol *5*.

Shen, K., and Meyer, T. (1999). Dynamic control of CaMKII translocation and localization in hippocampal neurons by NMDA receptor stimulation. Science *284*, 162-166.

Ster, J., Steuble, M., Orlando, C., Diep, T.M., Akhmedov, A., Raineteau, O., Pernet, V., Sonderegger, P., and Gerber, U. (2014). Calsyntenin-1 regulates targeting of dendritic NMDA receptors and dendritic spine maturation in CA1 hippocampal pyramidal cells during postnatal development. J Neurosci *34*, 8716-8727.

Steuble, M., Diep, T.M., Schatzle, P., Ludwig, A., Tagaya, M., Kunz, B., and Sonderegger, P. (2012). Calsyntenin-1 shelters APP from proteolytic processing during anterograde axonal transport. Biol Open *1*, 761-774.

Stowers, R.S., Megeath, L.J., Gorska-Andrzejak, J., Meinertzhagen, I.A., and Schwarz, T.L. (2002). Axonal transport of mitochondria to synapses depends on milton, a novel Drosophila protein. Neuron *36*, 1063-1077.

Summers, D.W., DiAntonio, A., and Milbrandt, J. (2014). Mitochondrial dysfunction induces Sarm1-dependent cell death in sensory neurons. J Neurosci *34*, 9338-9350.

Summers, D.W., Frey, E., Walker, L.J., Milbrandt, J., and DiAntonio, A. (2020). DLK Activation Synergizes with Mitochondrial Dysfunction to Downregulate Axon Survival Factors and Promote SARM1-Dependent Axon Degeneration. Mol Neurobiol *57*, 1146-1158.

Summers, D.W., Gibson, D.A., DiAntonio, A., and Milbrandt, J. (2016). SARM1-specific motifs in the TIR domain enable NAD^+ loss and regulate injury-induced SARM1 activation. Proc Natl Acad Sci U S A *113*, E6271-E6280.

Sure, G.R., Chatterjee, A., Mishra, N., Sabharwal, V., Devireddy, S., Awasthi, A., Mohan, S., and Koushika, S.P. (2018). UNC-16/JIP3 and UNC-76/FEZ1 limit the density of mitochondria in C. elegans neurons by maintaining the balance of anterograde and retrograde mitochondrial transport. Sci Rep *8*, 8938.

Takei, N., Sobu, Y., Kimura, A., Urano, S., Piao, Y., Araki, Y., Taru, H., Yamamoto, T., Hata, S., Nakaya, T., *et al.* (2015). Cytoplasmic fragment of Alcadein alpha generated by regulated intramembrane proteolysis enhances amyloid beta-protein precursor (APP) transport into the late secretory pathway and facilitates APP cleavage. J Biol Chem *290*, 987-995.

bioRxiv preprint doi: https://doi.org/10.1101/2021.09.12.459970; this version posted September 12, 2021. The copyright holder for this preprint (which was not certified by peer review) is the author/funder, who has granted bioRxiv a license to display the preprint in perpetuity. It is made available under aCC-BY-NC 4.0 International license.

Taylor, S.R., Santpere, G., Weinreb, A., Barrett, A., Reilly, M.B., Xu, C., Varol, E., Oikonomou, P., Glenwinkel, L., McWhirter, R.*, et al.* (2020). Molecular topography of an entire nervous system. bioRxiv, 2020.2012.2015.422897.

Thapliyal, S., Vasudevan, A., Dong, Y., Bai, J., Koushika, S.P., and Babu, K. (2018). The C-terminal of CASY-1/Calsyntenin regulates GABAergic synaptic transmission at the Caenorhabditis elegans neuromuscular junction. PLoS Genet *14*, e1007263.

Tomita, S., Ozaki, T., Taru, H., Oguchi, S., Takeda, S., Yagi, Y., Sakiyama, S., Kirino, Y., and Suzuki, T. (1999). Interaction of a neuron-specific protein containing PDZ domains with Alzheimer's amyloid precursor protein. J Biol Chem *274*, 2243-2254.

Turkiew, E., Falconer, D., Reed, N., and Hoke, A. (2017). Deletion of Sarm1 gene is neuroprotective in two models of peripheral neuropathy. J Peripher Nerv Syst *22*, 162-171.

Uchida, Y., and Gomi, F. (2016). The role of calsyntenin-3 in dystrophic neurite formation in Alzheimer's disease brain. Geriatrics & Gerontology International *16*, 43-50.

Umemura, T., Rapp, P., and Rongo, C. (2005). The role of regulatory domain interactions in UNC-43 CaMKII localization and trafficking. J Cell Sci *118*, 3327-3338.

Vagnoni, A., Perkinton, M.S., Gray, E.H., Francis, P.T., Noble, W., and Miller, C.C. (2012). Calsyntenin-1 mediates axonal transport of the amyloid precursor protein and regulates Abeta production. Hum Mol Genet *21*, 2845-2854.

Veriepe, J., Fossouo, L., and Parker, J.A. (2015). Neurodegeneration in C. elegans models of ALS requires TIR-1/Sarm1 immune pathway activation in neurons. Nat Commun *6*, 7319.

Vogt, L., Schrimpf, S.P., Meskenaite, V., Frischknecht, R., Kinter, J., Leone, D.P., Ziegler, U., and Sonderegger, P. (2001). Calsyntenin-1, a proteolytically processed postsynaptic membrane protein with a cytoplasmic calcium-binding domain. Mol Cell Neurosci *17*, 151-166.

Walker, L.J., Summers, D.W., Sasaki, Y., Brace, E.J., Milbrandt, J., and DiAntonio, A. (2017). MAPK signaling promotes axonal degeneration by speeding the turnover of the axonal maintenance factor NMNAT2. Elife *6*.

Waterhouse, A.M., Procter, J.B., Martin, D.M., Clamp, M., and Barton, G.J. (2009). Jalview Version 2--a multiple sequence alignment editor and analysis workbench. Bioinformatics *25*, 1189-1191.

West, A.E., Chen, W.G., Dalva, M.B., Dolmetsch, R.E., Kornhauser, J.M., Shaywitz, A.J., Takasu, M.A., Tao, X., and Greenberg, M.E. (2001). Calcium regulation of neuronal gene expression. Proc Natl Acad Sci U S A *98*, 11024-11031.

Woolums, B.M., McCray, B.A., Sung, H., Tabuchi, M., Sullivan, J.M., Ruppell, K.T., Yang, Y., Mamah, C., Aisenberg, W.H., Saavedra-Rivera, P.C.*, et al.* (2020). TRPV4 disrupts mitochondrial transport and causes axonal degeneration via a CaMKII-dependent elevation of intracellular Ca(2). Nat Commun *11*, 2679.

Yang, E., and Schulman, H. (1999). Structural examination of autoregulation of multifunctional calcium/calmodulin-dependent protein kinase II. J Biol Chem *274*, 26199-26208.

Yang, J., Wu, Z., Renier, N., Simon, D.J., Uryu, K., Park, D.S., Greer, P.A., Tournier, C., Davis, R.J., and Tessier-Lavigne, M. (2015). Pathological axonal death through a MAPK cascade that triggers a local energy deficit. Cell *160*, 161-176.

Zalcman, G., Federman, N., and Romano, A. (2018). CaMKII Isoforms in Learning and Memory: Localization and Function. Front Mol Neurosci *11*, 445.

Zeng, X., Ye, M., Resch, J.M., Jedrychowski, M.P., Hu, B., Lowell, B.B., Ginty, D.D., and Spiegelman, B.M. (2019). Innervation of thermogenic adipose tissue via a calsyntenin 3beta-S100b axis. Nature *569*, 229-235.

Zhao, Y., Song, E., Wang, W., Hsieh, C.H., Wang, X., Feng, W., Wang, X., and Shen, K. (2021). Metaxins are core components of mitochondrial transport adaptor complexes. Nat Commun *12*, 83.

bioRxiv preprint doi: https://doi.org/10.1101/2021.09.12.459970; this version posted September 12, 2021. The copyright holder for this preprint (which was not certified by peer review) is the author/funder, who has granted bioRxiv a license to display the preprint in perpetuity. It is made available under aCC-BY-NC 4.0 International license.

1050 Zuchner, S., Mersiyanova, I.V., Muglia, M., Bissar-Tadmouri, N., Rochelle, J., Dadali, E.L., Zappia, M.,
1051 Nelis, E., Patitucci, A., Senderek, J.*, et al.* (2004). Mutations in the mitochondrial GTPase mitofusin 2
1052 cause Charcot-Marie-Tooth neuropathy type 2A. Nat Genet *36*, 449-451.
1053 Zundorf, G., and Reiser, G. (2011). Calcium dysregulation and homeostasis of neural calcium in the
1054 molecular mechanisms of neurodegenerative diseases provide multiple targets for neuroprotection.
1055 Antioxid Redox Signal *14*, 1275-1288.

bioRxiv preprint doi: https://doi.org/10.1101/2021.09.12.459970; this version posted September 12, 2021. The copyright holder for this preprint (which was not certified by peer review) is the author/funder, who has granted bioRxiv a license to display the preprint in perpetuity. It is made available under a CC BY-NC-ND 4.0 International license.

Figure 1

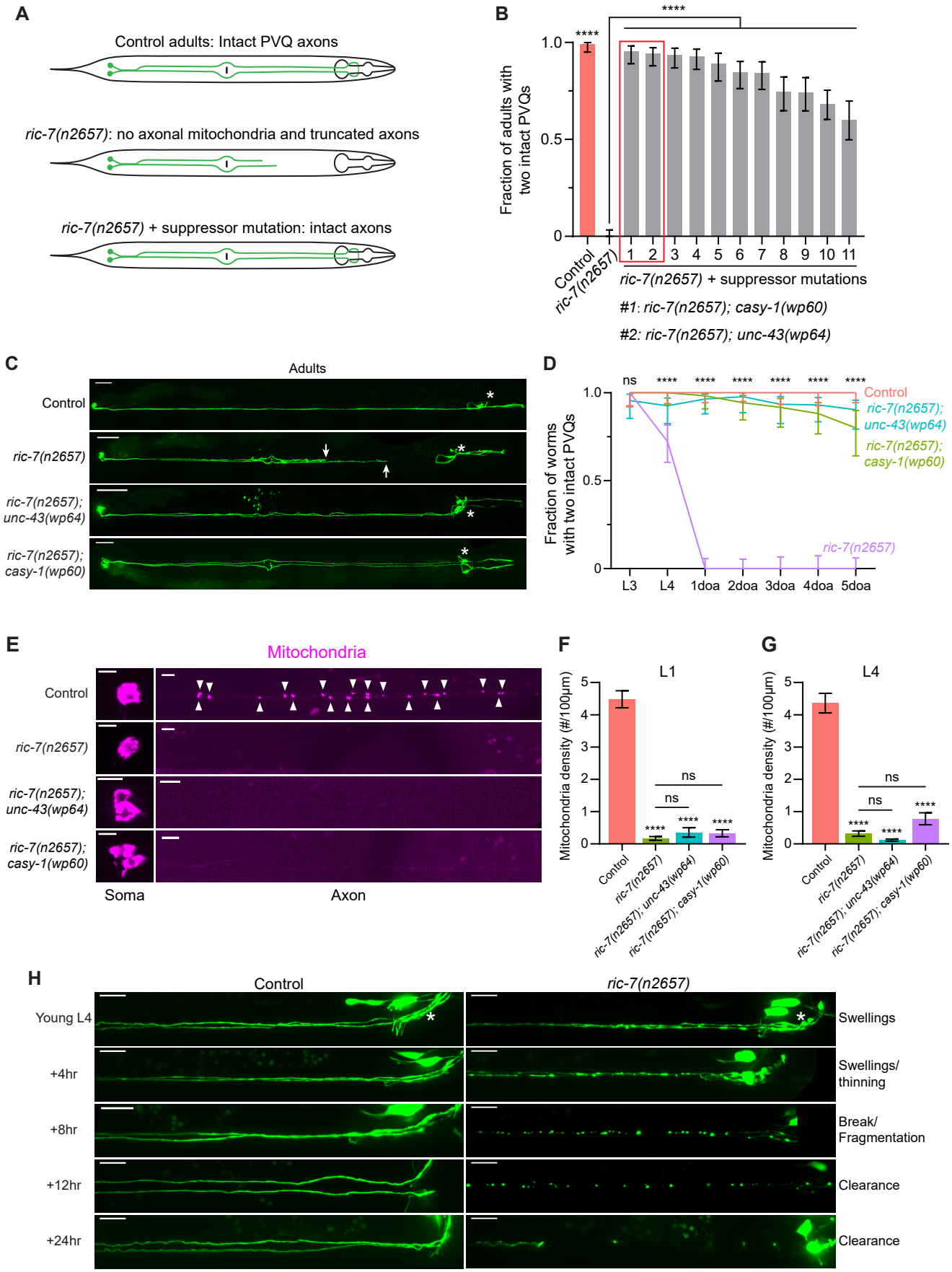

bioRxiv preprint doi: https://doi.org/10.1101/2021.09.12.459970; this version posted September 12, 2021. The copyright holder for this preprint (which was not certified by peer review) is the author/funder, who has granted bioRxiv a license to display the preprint in perpetuity. It is made available under aCC-BY-NC 4.0 International license.

Figure 1. An unbiased screen identifies suppressors of spontaneous axon degeneration caused by loss of mitochondria

(A) Diagrams of PVQ neurons in control, *ric-7(n2657)* and *ric-7(n2657)* + suppressor animals. Throughout this study, PVQ neurons are visualized with *oyIs14[sra-6p::GFP]*, and mitochondria in PVQ are visualized with *sra-6p::mito::TagRFP.*

(B) Axon degeneration modifiers identified in unbiased forward genetic screen. Graph shows proportion of 3-day-old adult (3doa) animals without degeneration in either PVQ neuron. Leftmost bars show control (99% animals without degeneration) and *ric-7(n2657)* (0% animals without degeneration). Remaining bars show strains that are all *ric-7(n2657)* mutants and that also carry an independent mutation that suppresses degeneration. The top two suppressor mutants, *ric-7(n2657); casy-1(wp60)* and *ric-7(n2657); unc-43(wp64)*, are highlighted. Bars show proportion and 95% confidence intervals (CI), N > 74 for all strains. **** indicates p<0.0001, compared to *ric-7(n2657)*, Fisher's exact test.

(C) Suppression of axon degeneration by mutations in CaMKII/*unc-43* and calsyntenin/*casy-1*. Representative images of control, *ric-7(n2657)*, *ric-7(n2657); unc-43(wp64)* and *ric-7(n2657); casy-1(wp60)* 2-3doa. Arrows indicate the tips of degenerated axons. Asterisks indicate the head neurons—these are co-labeled by the GFP reporter but are not the subject of this study. Scale bar, 50 µm.

(D) Quantification of suppression of axon degeneration. PVQ degeneration is analyzed from the L3 stage to 5doa in control and suppressor mutants. Graph shows proportion and 95% CI. N = 44-74 for each timepoint. **** indicates p<0.0001, ns = not significant, Chi-square test.

(E) Suppressors of degeneration do not restore axonal mitochondria. Images of mitochondria in PVQ neurons in control, *ric-7(n2657)*, and suppressor mutants at L4. Arrowheads indicate mitochondria in axons. Scale bar, 5 µm.

(F and G) Quantification of mitochondria density in control, *ric-7(n2657)*, and suppressor mutants at L1 and L4 stages. Bars show mean and SEM. N = 16, 26, 63, 53 for L1s and N = 54, 52, 50, 70 for L4s. **** indicates p<0.0001, ns = not significant, compared to control except where indicated, one-way ANOVA, Kruskal-Wallis test, followed by Dunn's multiple comparisons.

(H) Axon degeneration in the absence of mitochondria is progressive. Images of axon morphology in a single control and a single *ric-7(n2657)* animal at timepoints during the L4-1doa transition. Asterisk indicates the nerve ring. Scale bar, 10 µm.

bioRxiv preprint doi: https://doi.org/10.1101/2021.09.12.459970; this version posted September 12, 2021. The copyright holder for this preprint (which was not certified by peer review) is the author/funder, who has granted bioRxiv a license to display the preprint in perpetuity. It is made available under aCC-BY-NC-ND 4.0 International license.

Figure 2

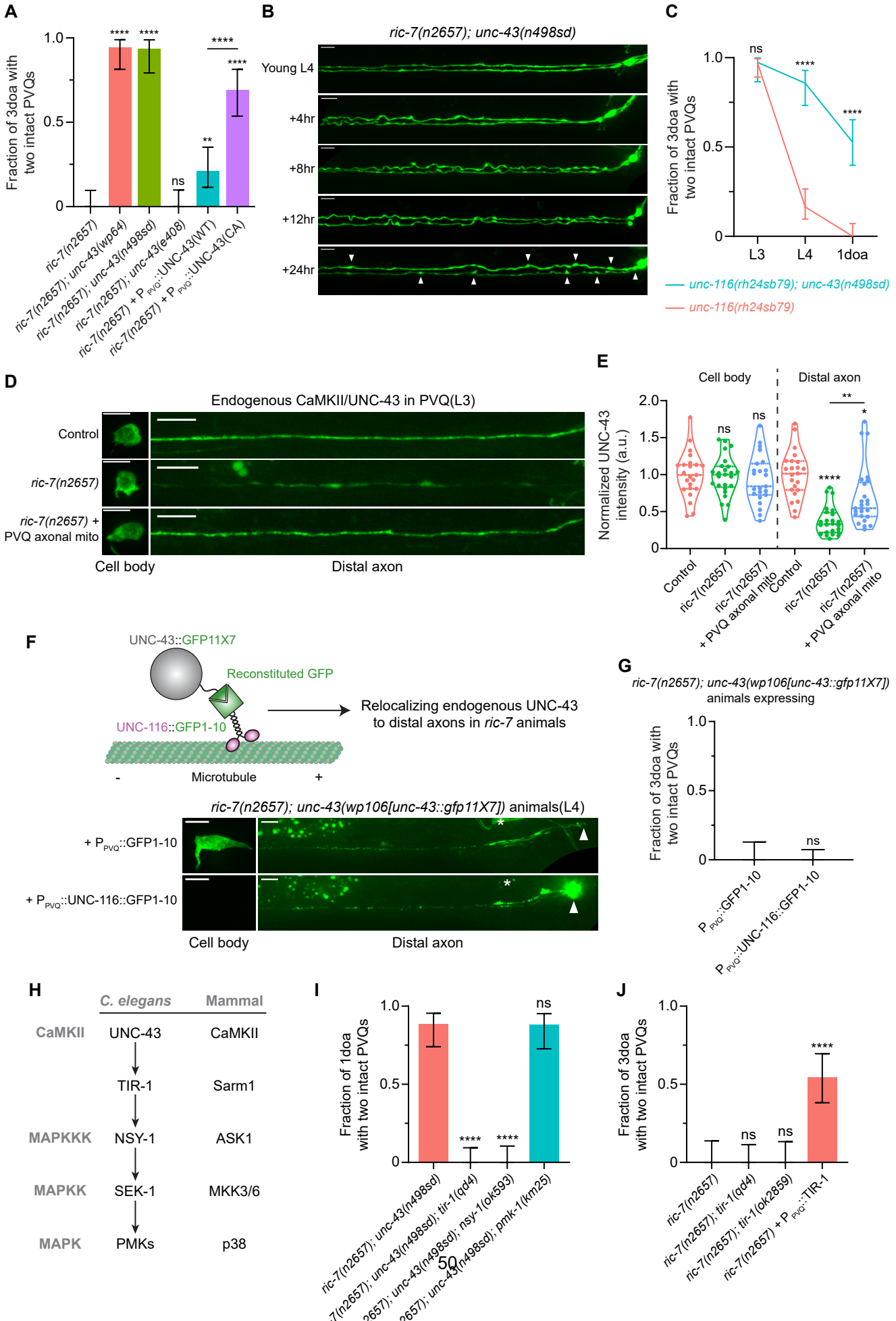

bioRxiv preprint doi: https://doi.org/10.1101/2021.09.12.459970; this version posted September 12, 2021. The copyright holder for this preprint (which was not certified by peer review) is the author/funder, who has granted bioRxiv a license to display the preprint in perpetuity. It is made available under aCC-BY-NC 4.0 International license.

Figure 2. Active CaMKII/UNC-43 suppresses axon degeneration cell autonomously through the conserved Sarm1/TIR-1-ASK1/NSY-1 MAPK pathway

(A) Active CaMKII/UNC-43 functions cell-autonomously to suppress degeneration. Quantification of axon degeneration in 3-day-old adult (3doa) animals. Genotypes and number of animals: *ric-7(n2657)* (N = 36), *ric-7(n2657); unc-43(wp64)* (N = 35), *ric-7(n2657); unc-43(n498sd)* (N = 31), *ric-7(n2657); unc-43(e408)* (N = 35), *ric-7(n2657)* + P_{PVQ}::WT UNC-43 (N = 43) and *ric-7(n2657)* + P_{PVQ}::constitutively-active (CA) UNC-43 (N = 39). Bars show proportion and 95% CI. **** indicates p<0.0001, ** indicates p<0.01, ns = not significant, compared to *ric-7(n2657)* except where indicated, Fisher's exact test.

(B) Images of axon morphology in a single *ric-7(n2657); unc-43(n498sd)* animal at timepoints during the L4-1doa transition. Arrowheads indicate axon swellings. Scale bar, 10 µm.

(C) Loss of kinesin-1/*unc-116* results in axon degeneration that is suppressed by active CaMKII/*unc-43*. Quantification of axon degeneration from the L3 stage to 1-day-old adults. Genotypes and number of animals: *unc-116(rh24sb79)* (N = 50-73), and *unc-116(rh24sb79); unc-43(n498sd)* (N = 38-55). Graph shows proportion and 95% CI. **** indicates p<0.0001, ns = not significant, compared to *unc-116(rh24sb79)*, Fisher's exact test.

(D) Endogenous CaMKII/UNC-43 localization. Images of NATF-tagged CaMKII/UNC-43 in PVQ cell bodies and distal axons adjacent to the nerve ring in control, *ric-7(n2657)*, and *ric-7(n2657)* + P_{PVQ}::UNC-116::TOMM-7 in L3 stage animals. Scale bar, 5 µm.

(E) Normalized NATF-tagged CaMKII/UNC-43 intensities (arbitrary units) in PVQ cell bodies and distal axons in control, *ric-7(n2657)* and *ric-7(n2657)* + P_{PVQ}::UNC-116::TOMM-7 in L3 stage animals. Violin plots with median and quantiles are shown. **** indicates p<0.0001, ** indicates p<0.01, * indicates p<0.05, ns = not significant, compared to control except where indicated, one-way ANOVA, Kruskal-Wallis test, followed by Dunn's multiple comparisons.

(F) Adapting the NATF approach to relocalize endogenous CaMKII/UNC-43 to distal axons. Images of endogenous CaMKII/UNC-43 in PVQ cell bodies and distal axons in *ric-7(n2657); unc-43(wp106[unc-43::gfp11X7])* animals that express P_{PVQ}::GFP1-10 or P_{PVQ}::UNC-116::GFP1-10 at the L4 stage. Arrowhead indicates axon tip. Asterisk indicates cell body of head neurons. Scale bar, 5 µm.

(G) Relocalizing endogenous CaMKII/UNC-43 to distal axons does not suppress degeneration in *ric-7(n2657)* animals. Quantification of axon degeneration in 3doa. Genotypes and number of animals: *ric-7(n2657); unc-43(wp106[unc-43::gfp11X7])* + P_{PVQ}::GFP1-10 (N = 26), and *ric-7(n2657); unc-43(wp106[unc-43::gfp11X7])* + P_{PVQ}::UNC-116::GFP1-10 (N = 48). Bars show proportion and 95% CI. ns = not significant, Fisher's exact test.

(H) The UNC-43-TIR-1-MAPK pathway and conservation in mammals.

(I) The TIR-1-NSY-1-MAPK pathway is required to suppress axon degeneration in activated CaMKII/*unc-43* mutants. Quantification of axon degeneration in 1doa. Genotypes and number of animals: *ric-7(n2657); unc-43(n498sd)* (N = 35), *ric-7(n2657); unc-43(n498sd); tir-1(qd4)* (N = 37), *ric-7(n2657); unc-43(n498sd); nsy-1(ok593)* (N = 33), and *ric-7(n2657); unc-43(n498sd), pmk-1(km25)* (N = 33). Bars show proportion and 95% CI. **** indicates p<0.0001, ns = not significant, compared to *ric-7(n2657); unc-43(n498sd)*, Fisher's exact test.

(J) Sarm1/TIR-1 protects against degeneration in the context of lack of axonal mitochondria. Quantification of axon degeneration in 3doa. Genotypes and number of animals: *ric-7(n2657)* (N = 24), *ric-7(n2657); tir-1(qd4)* (N = 30), *ric-7(n2657); tir-1(ok2859)* (N = 25) and *ric-7(n2657)* + P_{PVQ}::WT TIR-1 (N = 35). Bars show proportion and 95% CI. **** indicates p<0.0001, ns = not significant, compared to *ric-7(n2657)*, Fisher's exact test.

bioRxiv preprint doi: https://doi.org/10.1101/2021.09.12.459970; this version posted September 12, 2021. The copyright holder for this preprint (which was not certified by peer review) is the author/funder, who has granted bioRxiv a license to display the preprint in perpetuity. It is made available under aCC BY-NC-ND 4.0 International license.

Figure 3

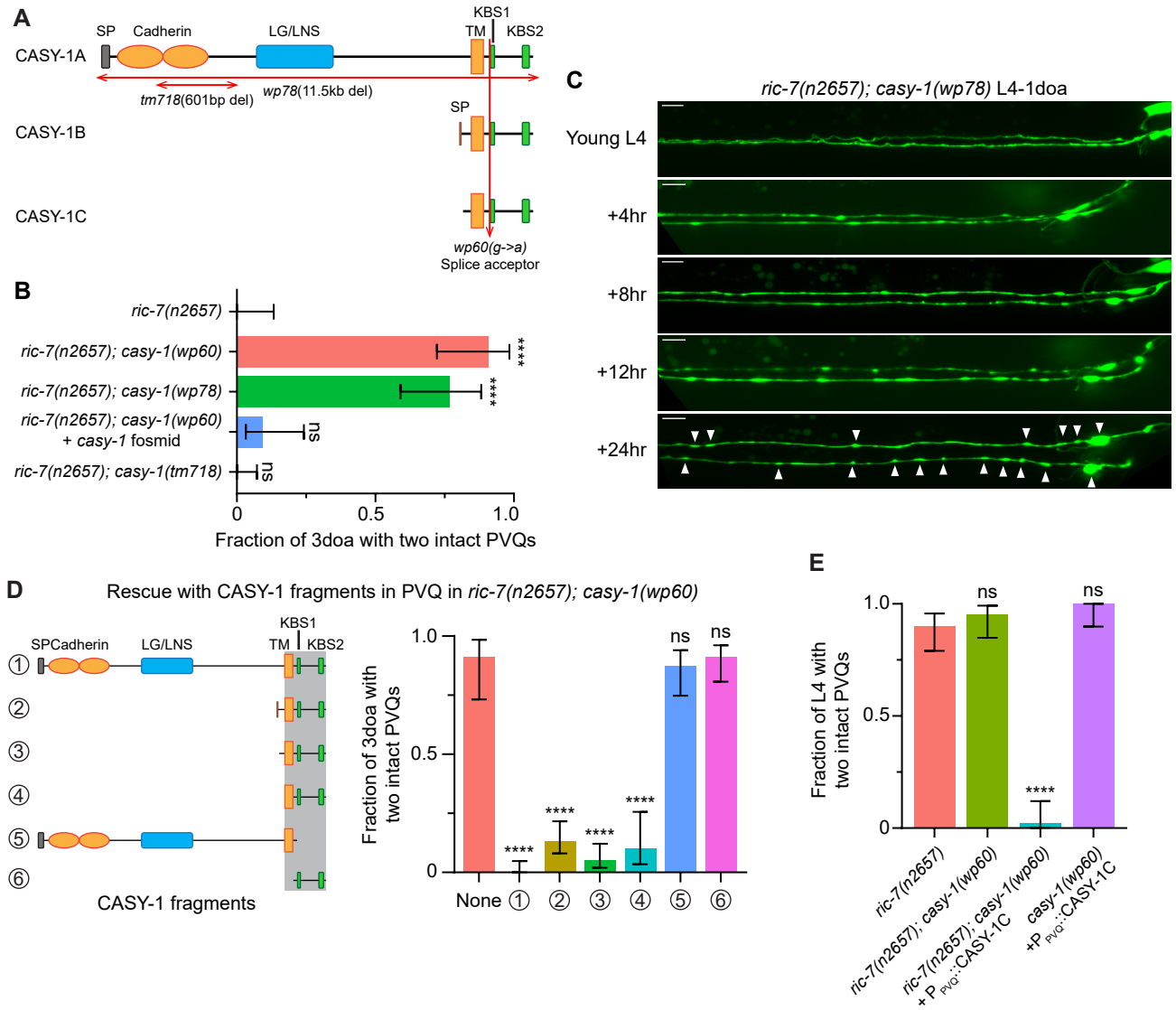

Figure 3. Calsyntenin/CASY-1 promotes axon degeneration cell autonomously

(A) The three C. elegans CASY-1 isoforms. SP, signal peptide; LG/LNS, laminin G-like; TM, transmembrane domain; KBS, kinesin-binding site.

(B) Loss of calsyntenin/casy-1 suppresses degeneration due to loss of axonal mitochondria. Quantification of axon degeneration in 3doa. Genotypes and number of animals: *ric-7(n2657)* (N = 25), *ric-7(n2657); casy-1(wp60)* (N = 22), *ric-7(n2657); casy-1(wp78)* (N = 30), *ric-7(n2657); casy-1(wp60)* + the *casy-1* fosmid WRM0622dH03 (N = 32), and *ric-7(n2657); casy-1(tm718)* (N = 49). Bars show proportion and 95% CI. **** indicates p<0.0001, ns = not significant, compared to *ric-7(n2657)*, Fisher's exact test.

(C) Loss of calsyntenin/*casy-1* arrests degeneration before axon severing. Images of axon morphology in a *ric-7(n2657); casy-1(wp78)* animal during the L4-1doa transition. Arrowheads indicate axon swellings. Scale bar, 10 µm.

(D) Structure-function analysis of CASY-1. Left, six CASY-1 fragments expressed in PVQ in *ric-7(n2657); casy-1(wp60)* animals. Right, quantification of axon degeneration in 3doa. Number of animals in experiments, respectively: 23, 76, 97, 80, 30, 47 and 56. Bars show proportion and 95% CI. **** indicates p<0.0001, ns = not significant, compared to *ric-7(n2657); casy-1(wp60)* with no transgene, Fisher's exact test. Transgenic fragments #1-4 restore degeneration to *ric-7(n2657); casy-1(wp60)* mutants.

(E) Overexpression of calsyntenin/*casy-1* enhances axon degeneration due to loss of axonal mitochondria. Quantification of axon degeneration in L4 stage animals. Genotypes and number of animals: *ric-7(n2657)* (N = 51), *ric-7(n2657); casy-1(wp60)* (N = 44), *ric-7(n2657); casy-1(wp60)* + P_{PVQ}::CASY-1C (N = 43), and *casy-1(wp60)* + P_{PVQ}::CASY-1C (N = 34). Bars show proportion and 95% CI. **** indicates p<0.0001, ns = not significant, compared to *ric-7(n2657)*, Fisher's exact test.

bioRxiv preprint doi: https://doi.org/10.1101/2021.09.12.459970; this version posted September 12, 2021. The copyright holder for this preprint (which was not certified by peer review) is the author/funder, who has granted bioRxiv a license to display the preprint in perpetuity. It is made available under a CC-BY-NC-ND 4.0 International license.

Figure 4

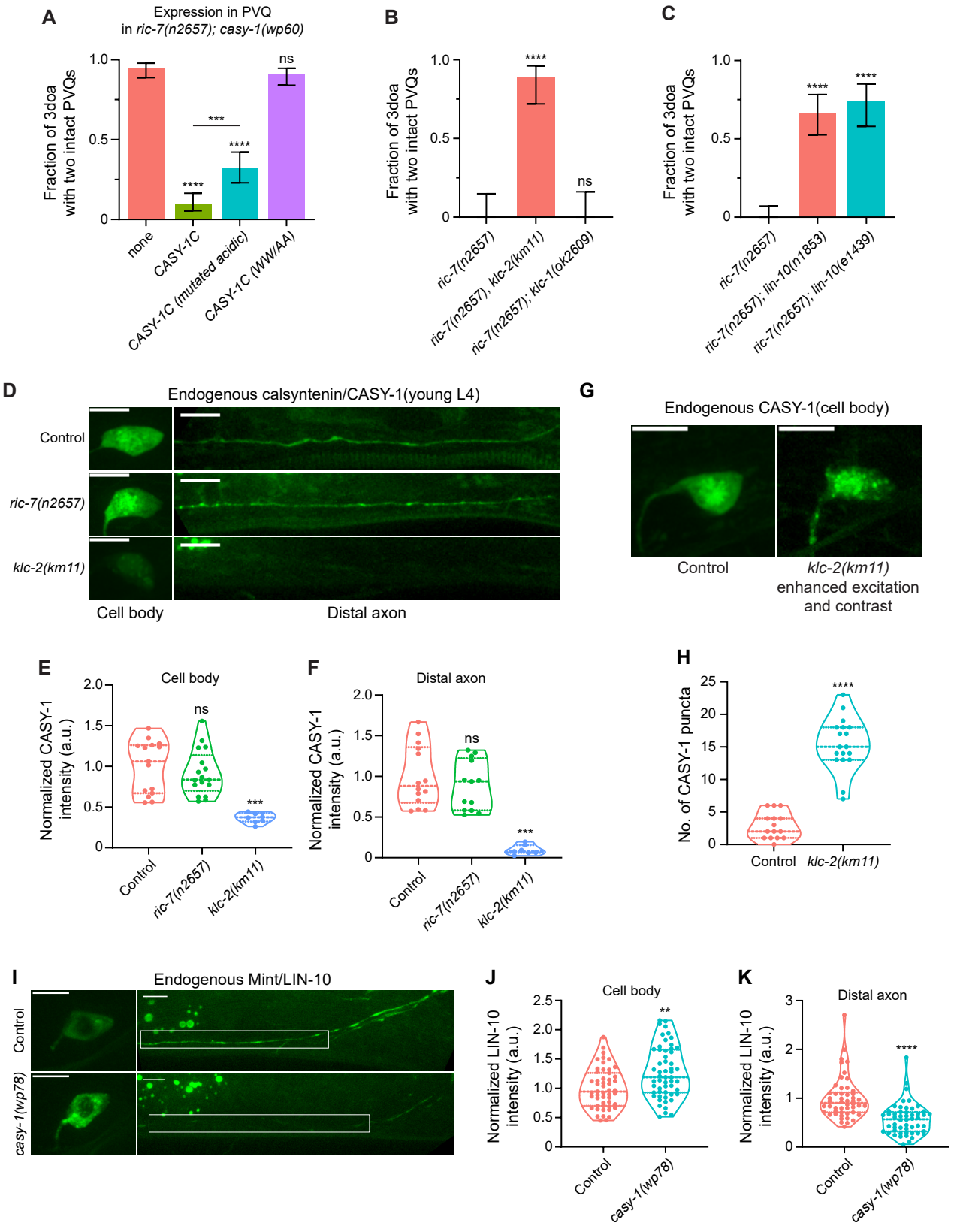

bioRxiv preprint doi: https://doi.org/10.1101/2021.09.12.459970; this version posted September 12, 2021. The copyright holder for this preprint (which was not certified by peer review) is the author/funder, who has granted bioRxiv a license to display the preprint in perpetuity. It is made available under aCC-BY-NC 4.0 International license.

Figure 4. Calsyntenin/CASY-1 functions as a kinesin adaptor for Mint/LIN-10 to promote axon degeneration

(A) Kinesin binding is required for calsyntenin's function in axon degeneration. Quantification of axon degeneration in 3doa. All animals have the *ric-7(n2657); casy-1(wp60)* background. Transgenes and number of animals: None (control) (N = 100); WT CASY-1C (N = 114); CASY-1C with mutated acidic residues (N = 88); CASY-1C with the WW/AA mutation (N = 118). Bars show proportion and 95% CI. **** indicates p<0.0001, *** indicates p<0.001, ns = not significant, compared to *ric-7(n2657); casy-1(wp60)* with no transgene except where indicated, Fisher's exact test. Transgenic CASY-1C with the WW/AA mutation does not restore degeneration to *ric-7(n2657); casy-1(wp60)* mutants.

(B) Loss of kinesin light chain *klc-2* suppresses axon degeneration. Quantification of axon degeneration in 3doa. Genotypes and number of animals: *ric-7(n2657)* (N = 22), *ric-7(n2657), klc-2(km11)* (N = 27), and *ric-7(n2657); klc-1(ok2609)* (N = 20). Bars show proportion and 95% CI. **** indicates p<0.0001, ns = not significant, compared to *ric-7(n2657)*, Fisher's exact test.

(C) Loss of Mint/*lin-10* suppresses axon degeneration. Quantification of axon degeneration in 3doa. Genotypes and number of animals: *ric-7(n2657)* (N = 50), *ric-7(n2657); lin-10(n1853)* (N = 48), and *ric-7(n2657); lin-10(e1439)* (N = 38). Bars show proportion and 95% CI. **** indicates p<0.0001, compared to *ric-7(n2657)*, Fisher's exact test.

(D) Images of NATF-tagged calsyntenin/CASY-1 in PVQ cell bodies and distal axons in control, *ric-7(n2657)*, and *klc-2(km11)* animals at early L4 stage. Scale bar, 5 µm.

(E) and **(F)** Loss of kinesin light chain *klc-2* alters calsyntenin abundance. Normalized NATF-tagged CASY-1 intensities (arbitrary units) in PVQ cell bodies and distal axons. Violin plots with median and quantiles are shown. *** indicates p<0.001, ns = not significant, compared to control, one-way ANOVA, Kruskal-Wallis test, followed by Dunn's multiple comparisons.

(G) Calsyntenin accumulates in cell body puncta in animals that lack kinesin light chain *klc-2*. Images of NATF-tagged CASY-1 in PVQ cell bodies in control and *klc-2(km11)* at early L4 stage. Excitation and contrast are enhanced in *klc-2(km11)* animals. Scale bar, 5 µm.

(H) Number of NATF-tagged CASY-1 puncta in PVQ cell bodies. Violin plots with median and quantiles are shown. **** indicates p<0.0001, compared to control, Mann-Whitney test.

(I) Images of NATF-tagged Mint/LIN-10 in PVQ cell bodies and distal axons in control and *casy-1(wp78)* animals at L4 stage. Boxes highlight the distal axon region for quantifications in (K). Scale bar, 5 µm.

(J) and **(K)** Mint/LIN-10 is depleted from distal axon in animals that lack calsyntenin. Normalized NATF-tagged LIN-10 intensities (arbitrary units) in PVQ cell bodies and distal axons. Violin plots with median and quantiles are shown. **** indicates p<0.0001, ** indicates p<0.01, compared to control, Mann-Whitney test.

bioRxiv preprint doi: https://doi.org/10.1101/2021.09.12.459970; this version posted September 12, 2021. The copyright holder for this preprint (which was not certified by peer review) is the author/funder, who has granted bioRxiv a license to display the preprint in perpetuity. It is made available under a CC-BY-NC-ND 4.0 International license.

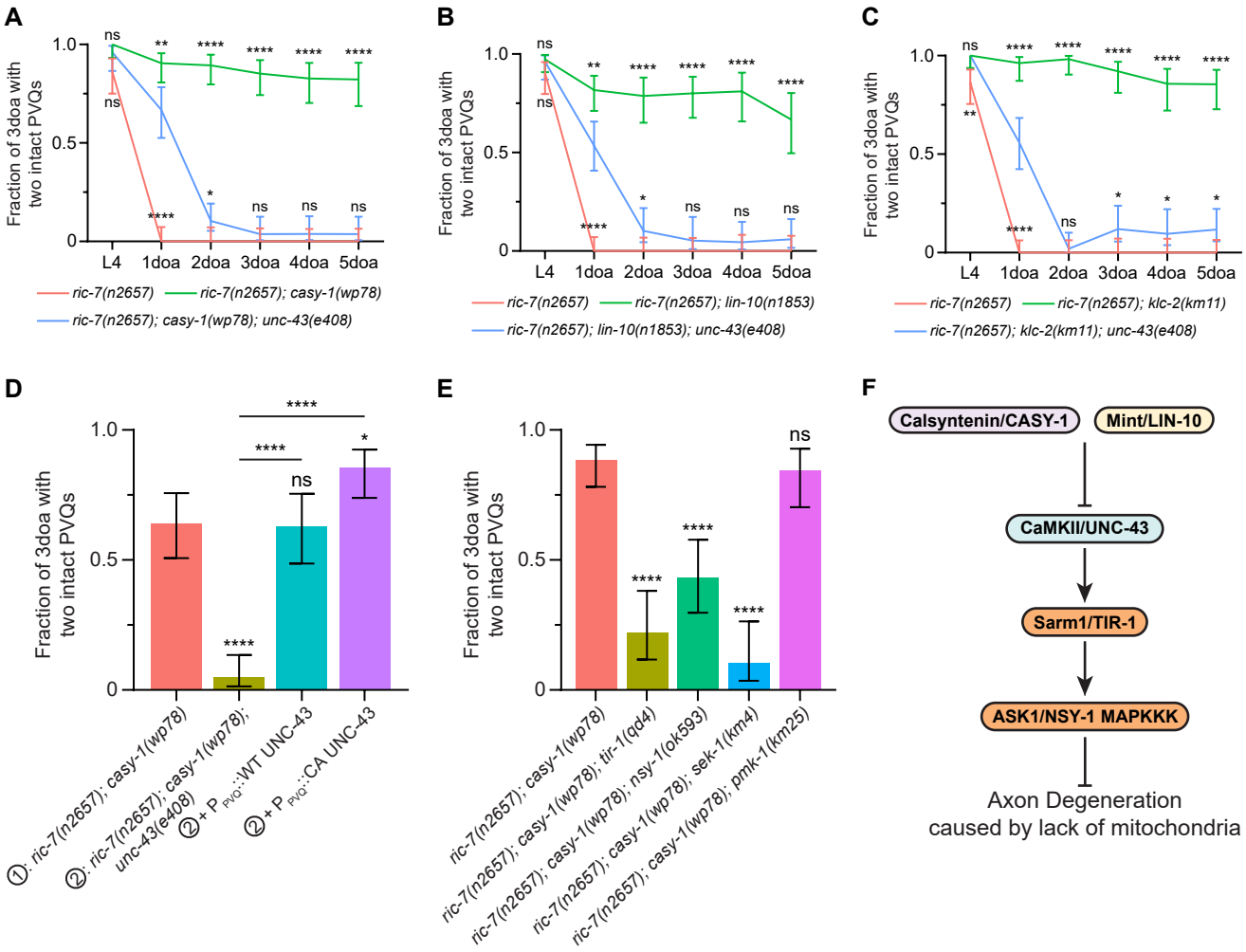

Figure 5. Loss of calsyntenin/CASY-1 or Mint/LIN-10 suppresses axon degeneration by activating the CaMKII-Sarm1-ASK1 MAPK pathway

(A-C) Axon protection conferred by loss of calsyntenin/*casy-1* requires CaMKII (A), Mint (B), and kinesin (C). Quantification of axon degeneration from L4 to 5doa. Number of animals: 45-77 (A), 33-75 (B), 42-60 (C). animals. Graphs show proportion and 95% CI. **** indicates p<0.0001, ** indicates p<0.01, * indicates p<0.05, ns = not significant, compared to the triple mutant (blue curve) at each timepoint, Fisher's exact test.

(D) CaMKII/*unc-43* is required cell-autonomously to suppress axon degeneration in calsyntenin/*casy-1* mutants. Quantification of axon degeneration in 3doa. Genotypes and number of animals: *ric-7(n2657); casy-1(wp78)* (N = 53), *ric-7(n2657); casy-1(wp78); unc-43(e408)* (N = 61), and *ric-7(n2657); casy-1(wp78); unc-43(e408)* + P_{PVQ}::WT UNC-43 (N = 46) or CA UNC-43 (N = 55). Bars show proportion and 95% CI. **** indicates p<0.0001, * indicates p<0.05, ns = not significant, compared to *ric-7(n2657); casy-1(wp78)* except where indicated, Fisher's exact test.

(E) The TIR-1-NSY-1-MAPK pathway is required to suppress axon degeneration in calsyntenin/*casy-1* mutants. Suppression of protection against axon degeneration in *ric-7(n2657); casy-1(wp78)* (N = 61) by *tir-1(qd4)* (N = 36), *nsy-1(ok593)* (N = 54), *sek-1(km4)* (N = 29), and *pmk-1(km25)* (N = 39). Bars show proportion and 95% CI. **** indicates p<0.0001, ns = not significant, compared to *ric-7(n2657); casy-1(wp78)*, Fisher's exact test.

(F) Diagram of regulation of axon degeneration by the calsyntenin-Mint-CaMKII-Sarm1-ASK1 MAPK pathway.

bioRxiv preprint doi: https://doi.org/10.1101/2021.09.12.459970; this version posted September 12, 2021. The copyright holder for this preprint (which was not certified by peer review) is the author/funder, who has granted bioRxiv a license to display the preprint in perpetuity. It is made available under aCC-BY-NC-ND 4.0 International license.

Figure 6

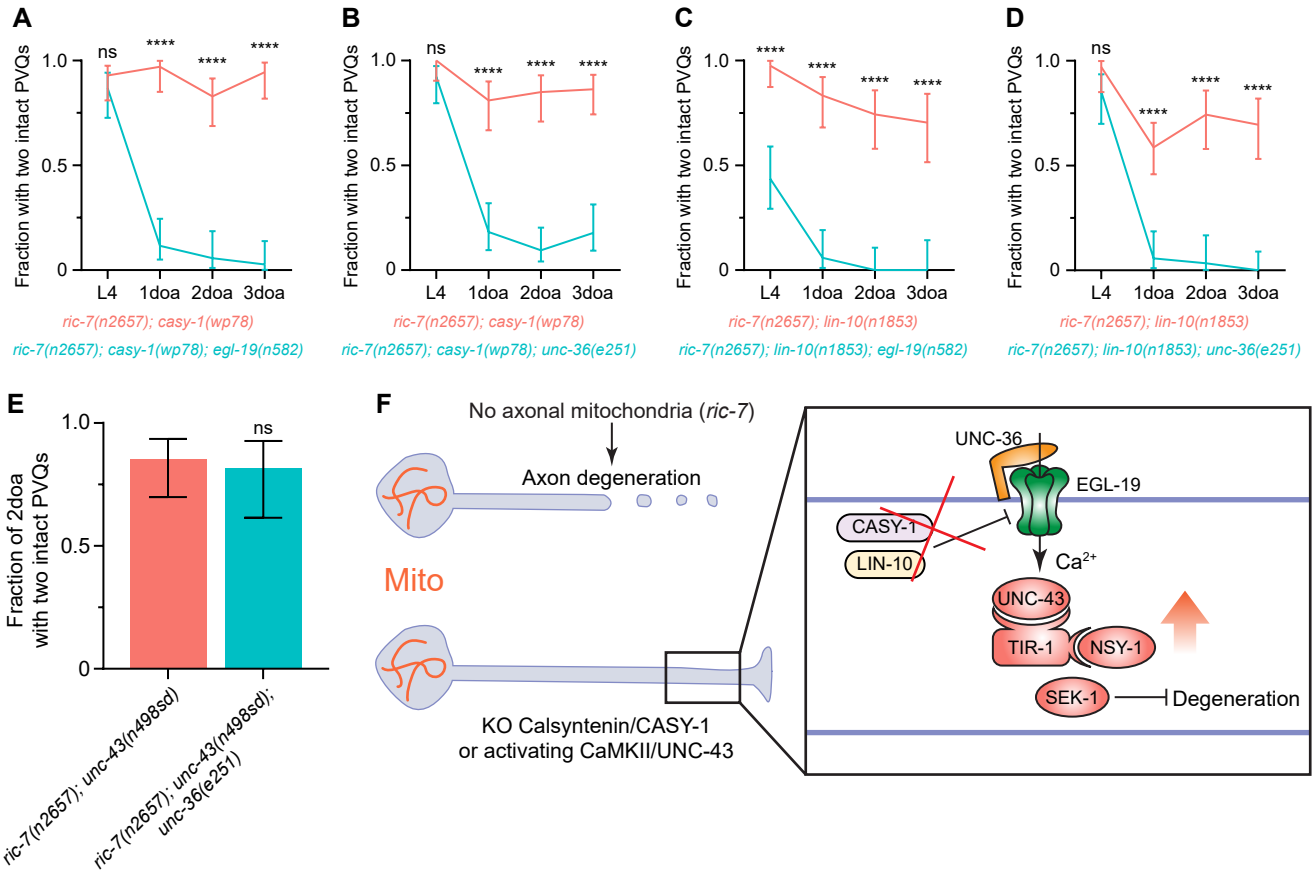

Figure 6. Loss of calsyntenin/CASY-1 or Mint/LIN-10 activates CaMKII/UNC-43 through the L-type voltage-gated calcium channel to suppress axon degeneration

(A-D) Axon protection conferred by loss of calsyntenin/*casy-1* or Mint/*lin-10* requires VGCC subunit *egl-19* (A, C) and VGCC subunit *unc-36* (B, D). Quantification of axon degeneration from L4 to 3doa. Number of animals = 27-58. Graphs show proportion and 95% CI. **** indicates p<0.0001 at each timepoint, ns = not significant, Fisher's exact test.

(E) Axon protection conferred by activation of CaMKII does not requires VGCC subunit *unc-36*. Quantification of axon degeneration in 2doa. Genotypes and number of animals: *ric-7(n2657); unc-43(n498sd)* (N = 34) and *ric-7(n2657); unc-43(n498sd); unc-36(e251)* (N = 22). Bars show proportion and 95% CI. ns = not significant, Fisher's exact test.

(F) Integrated model of how loss of calsyntenin/*casy-1* and Mint/*lin-10* suppress axon degeneration caused by the absence of mitochondria.

bioRxiv preprint doi: https://doi.org/10.1101/2021.09.12.459970; this version posted September 12, 2021. The copyright holder for this preprint (which was not certified by peer review) is the author/funder, who has granted bioRxiv a license to display the preprint in perpetuity. It is made available under a CC-BY-NC-ND 4.0 International license.

Figure 1-figure supplement 1

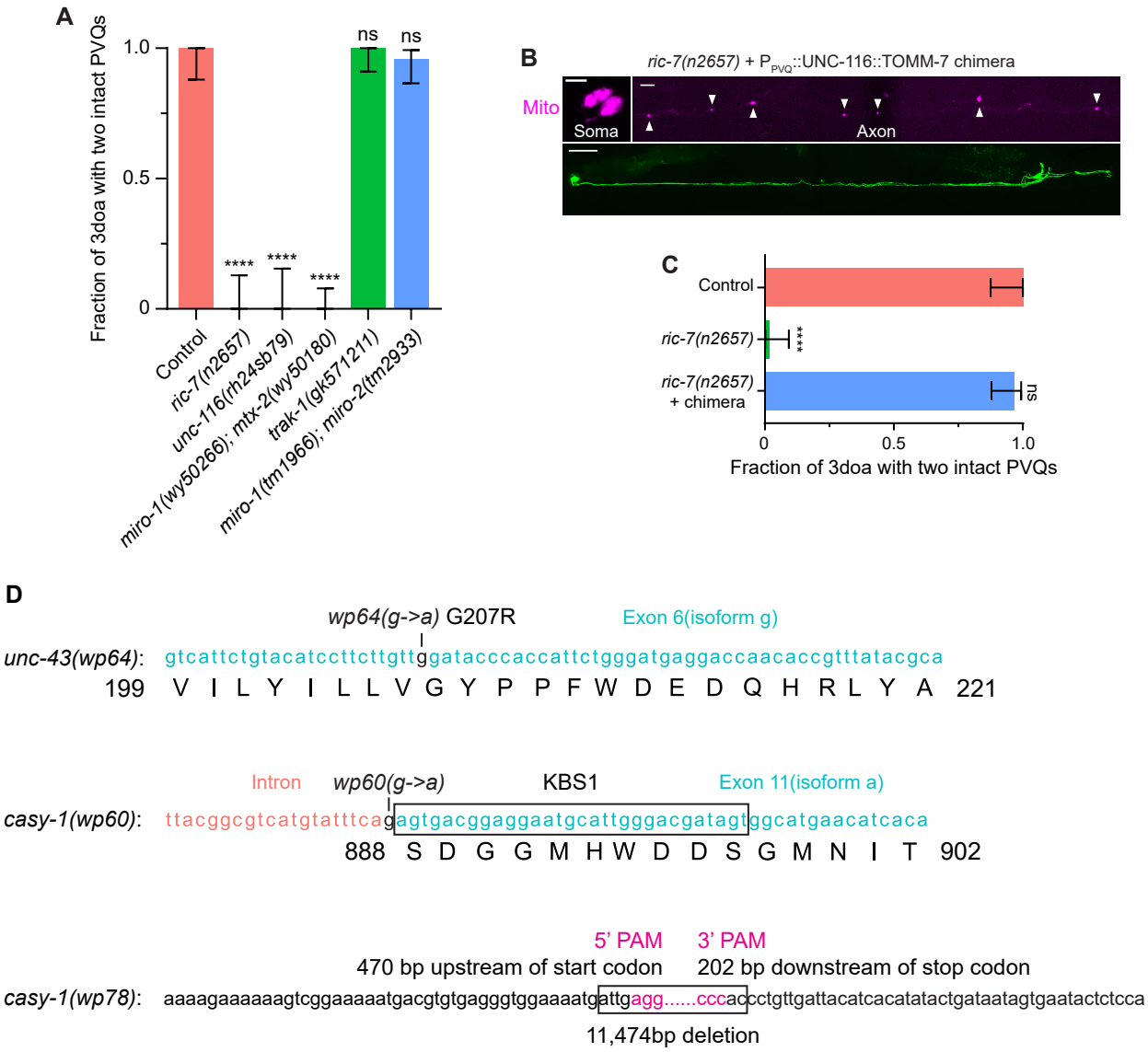

Figure 1-figure supplement 1. Complete loss of axonal mitochondria leads to degeneration and key allele information

(A) Axon degeneration in mutants of the mitochondria transport machinery. Quantification of axon degeneration in control (N = 28), *ric-7(n2657)* (N = 26), *unc-116(rh24sb79)* (N = 21), *miro-1(wy50266); mtx-2(wy50180)* (N = 45), *trak-1(gk571211)* (N = 39) and *miro-1(tm1966); miro-2(tm2933)* (N = 50) 3doa. Bars show proportion and 95% CI. **** indicates p<0.0001, ns = not significant, Fisher's exact test.

(B) Images of restored axonal mitochondria and suppressed degeneration in a *ric-7(n2657)* mutant that expresses the UNC-116::TOMM-7 chimera in PVQ. Scale bar, 5 µm for mitochondria and 50 µm for whole animal.

(C) Axon degeneration in *ric-7(n2657)* is due to loss of axonal mitochondria. Quantification of axon degeneration in control (N = 27), *ric-7(n2657)* (N = 57) and *ric-7(n2657)* with the UNC-116::TOMM-7 chimera in PVQ (N = 56). Bars show proportion and 95% CI. **** indicates p<0.0001, ns = not significant, Fisher's exact test.

(D) Detailed molecular information of key *unc-43* and *casy-1* alleles.

bioRxiv preprint doi: https://doi.org/10.1101/2021.09.12.459970; this version posted September 12, 2021. The copyright holder for this preprint (which was not certified by peer review) is the author/funder, who has granted bioRxiv a license to display the preprint in perpetuity. It is made available under a CC-BY-NC-ND 4.0 International license.

Figure 1-figure supplement 2

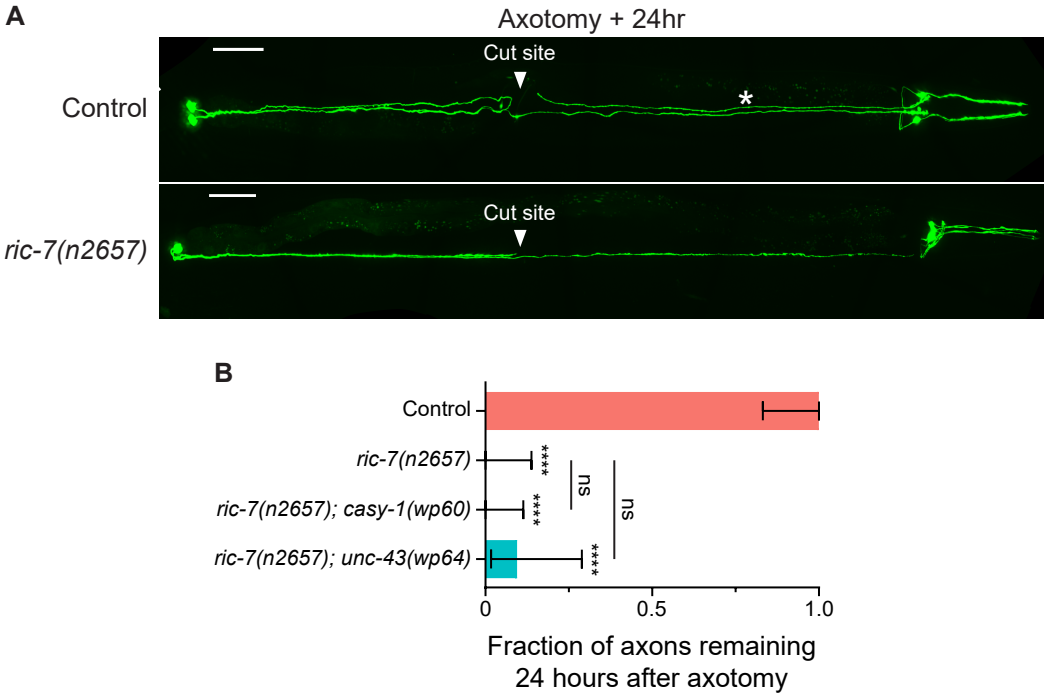

Figure 1-figure supplement 2. *casy-1(wp60)* and *unc-43(wp64)* do not suppress enhanced injury-induced axon degeneration (after laser axotomy) in *ric-7(n2657)*
(A) Representative images of laser axotomy-induced axon degeneration in PVQ in control and *ric-7(n2657)* animals. Asterisk indicates the remaining distal axon segment after axotomy.
(B) Quantification of the presence of the distal axon segments 24 hours after axotomy in control (N = 19), *ric-7(n2657)* (N = 24), *ric-7(n2657); casy-1(wp60)* (N = 30), and *ric-7(n2657); unc-43(wp64)* (N = 21) animals. Bars show proportion and 95% CI. **** indicates p<0.0001, ns = not significant, compared to control except where indicated, Fisher's exact test.

bioRxiv preprint doi: https://doi.org/10.1101/2021.09.12.459970; this version posted September 12, 2021. The copyright holder for this preprint (which was not certified by peer review) is the author/funder, who has granted bioRxiv a license to display the preprint in perpetuity. It is made available under a CC-BY-NC-ND 4.0 International license.

Figure 2-figure supplement 1

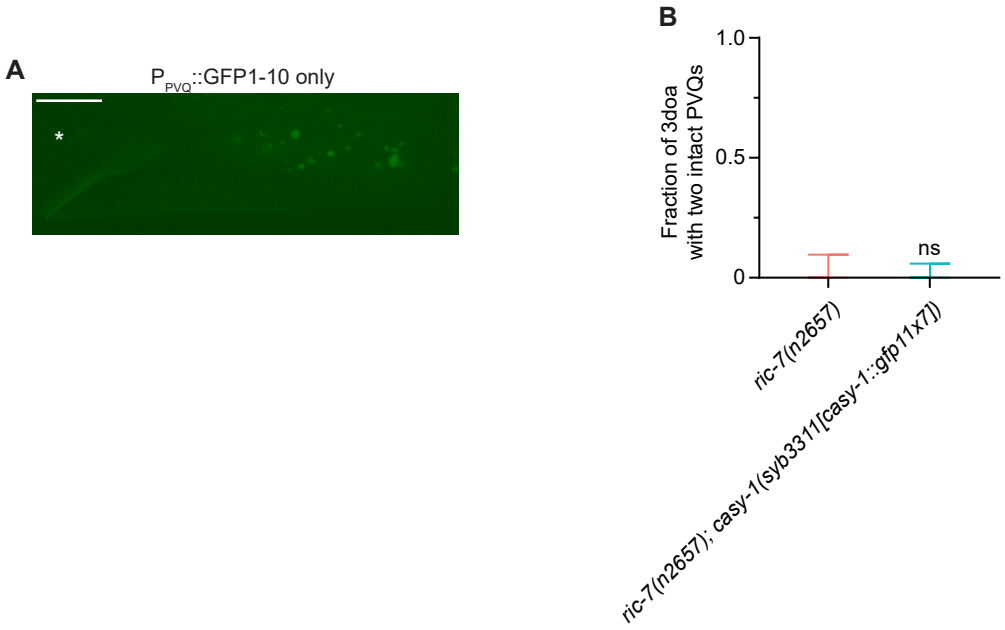

Figure 2-figure supplement 1. The GFP1-10 control and the *casy-1::gfp11x7* control for the NATF approach

(A) The P$_{PVQ}$::GFP1-10 construct alone has no detectable fluorescence. Asterisk indicates the approximate location of PVQ cell bodies.

(B) The NATF tag does not disrupt the function of calsyntenin/*casy-1* in axon degeneration. Quantification of axon degeneration in *ric-7(n2657)* (N = 36) and *ric-7(n2657); casy-1(syb3311[casy-1::gfp11x7])* (N = 63) 3doa. Bars show proportion and 95% CI. ns = not significant, Fisher's exact test.

bioRxiv preprint doi: https://doi.org/10.1101/2021.09.12.459970; this version posted September 12, 2021. The copyright holder for this preprint (which was not certified by peer review) is the author/funder, who has granted bioRxiv a license to display the preprint in perpetuity. It is made available under a CC-BY-NC-ND 4.0 International license.

Figure 4-figure supplement 1

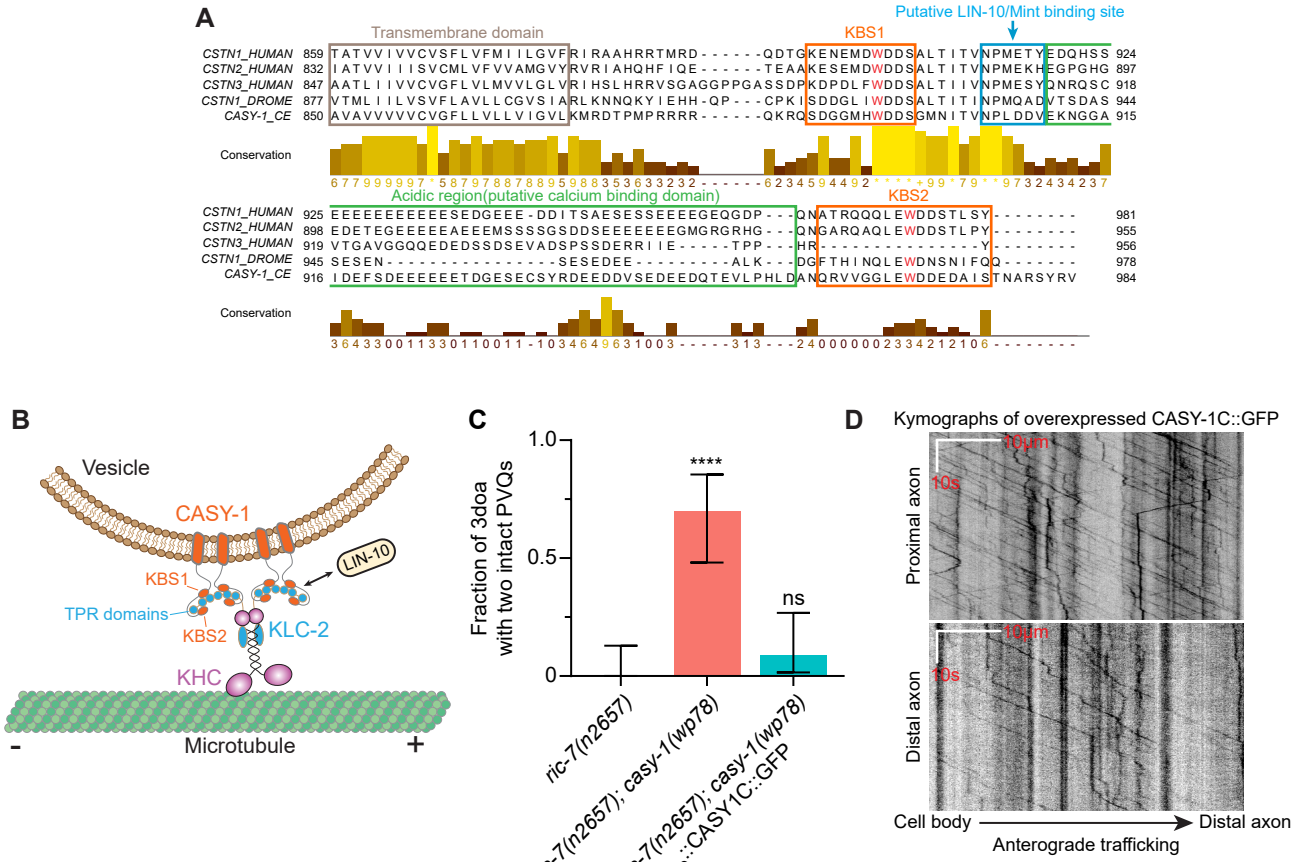

bioRxiv preprint doi: https://doi.org/10.1101/2021.09.12.459970; this version posted September 12, 2021. The copyright holder for this preprint (which was not certified by peer review) is the author/funder, who has granted bioRxiv a license to display the preprint in perpetuity. It is made available under aCC-BY-NC 4.0 International license.

Figure 4-figure supplement 1. Functional domains in the CASY-1 ICD and quantification of CASY-1C traffic

(A) Sequence alignment of the transmembrane and intracellular portion of *C. elegans*, *Drosophila* and human calsyntenins. The two tryptophan residues critical for KLC binding are highlighted in red.

(B) Model of how CASY-1 functions as a kinesin adaptor that transports cargoes such as Mint/LIN-10. KHC, kinesin heavy chain; TPR, tetratricopeptide repeat.

(C) GFP-tagged CASY-1C functions in axon degeneration. Quantification of axon degeneration in *ric-7(n2657)* (N = 26), *ric-7(n2657); casy-1(wp78)* (N = 20), and *ric-7(n2657); casy-1(wp78)* + P_{PVQ}::CASY-1C::GFP (N = 23) 3doa. Bars show proportion and 95% CI. **** indicates p<0.0001, ns = not significant, Fisher's exact test.

(D) Representative kymographs of trafficking of overexpressed CASY-1C::GFP in PVQ axons in *casy-1(wp78)* animals.

(E) Percentage of anterograde events of overexpressed CASY-1C::GFP in distal axons in *casy-1(wp78)* (N = 3491) and *ric-7(n2657); casy-1(wp78)* (N = 1233) animals at L4. Bars show proportion and 95% CI. **** indicates p<0.0001, Fisher's exact test.

(F) Speeds of CASY-1 vesicles in distal axons in *casy-1(wp78)* and *ric-7(n2657); casy-1(wp78)* (non-truncated axons) at L4. N = 1125 for *casy-1(wp78)* anterograde, 604 for *ric-7(n2657); casy-1(wp78)* anterograde, 262 for *casy-1(wp78)* retrograde, and 353 for *ric-7(n2657); casy-1(wp78)* retrograde. Box plots with whiskers are shown. **** indicates p<0.0001, unpaired t test.

(G) Run lengths of CASY-1 vesicles in distal axons in *casy-1(wp78)* and *ric-7(n2657); casy-1(wp78)* (non-truncated axons) at L4. N = 1125 for *casy-1(wp78)* anterograde, 604 for *ric-7(n2657); casy-1(wp78)* anterograde, 262 for *casy-1(wp78)* retrograde, and 353 for *ric-7(n2657); casy-1(wp78)* retrograde. Box plots with whiskers are shown. **** indicates p<0.0001, unpaired t test.

bioRxiv preprint doi: https://doi.org/10.1101/2021.09.12.459970; this version posted September 12, 2021. The copyright holder for this preprint (which was not certified by peer review) is the author/funder, who has granted bioRxiv a license to display the preprint in perpetuity. It is made available under a CC-BY-NC-ND 4.0 International license.

Figure 5-figure supplement 1

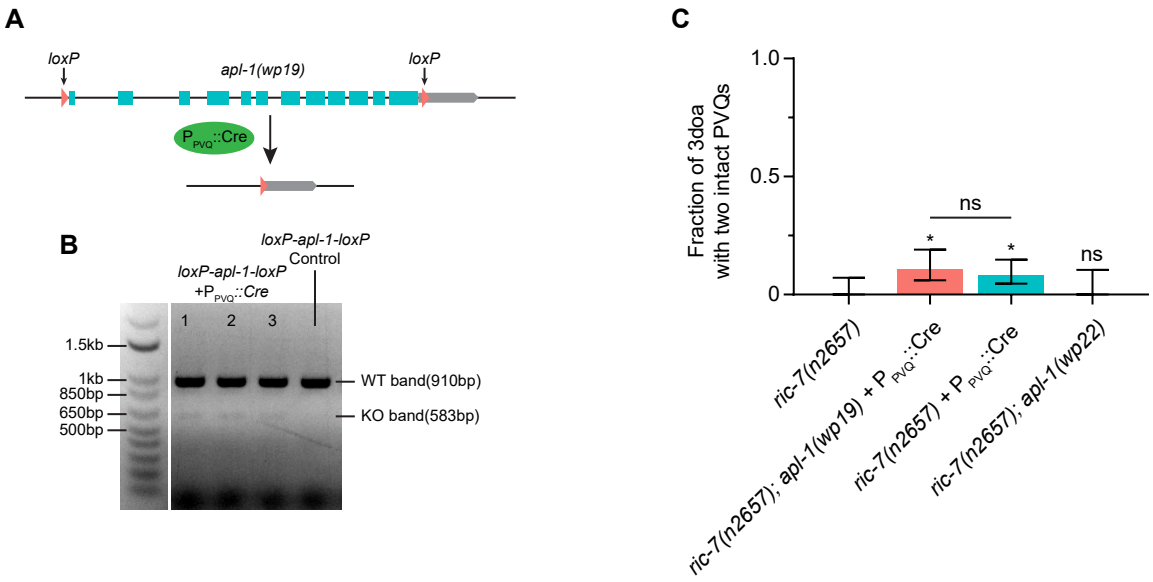

Figure 5-figure supplement 1. APL-1 mutations do not suppress spontaneous degeneration in *ric-7(n2657)*

(A) Schematic of the Cre-loxP method to knock out the entire *apl-1* gene in PVQ.

(B) Gel image showing the KO bands in three individual animals that express Cre in PVQ. The loxP control without Cre expression only shows the WT band.

(C) Quantification of axon degeneration in *ric-7(n2657)* (N = 50), *ric-7(n2657); apl-1(wp19)* + P_{PVQ}::Cre (N = 91), *ric-7(n2657)* + P_{PVQ}::Cre (N = 119), and *ric-7(n2657); apl-1(wp22)* (N = 33) 3doa. Mean and 95% CI are plotted. Bars show proportion and 95% CI. * indicates $p<0.05$, ns = not significant, compared to *ric-7(n2657)* except where indicated, Fisher's exact test.

bioRxiv preprint doi: https://doi.org/10.1101/2021.09.12.459970; this version posted September 12, 2021. The copyright holder for this preprint (which was not certified by peer review) is the author/funder, who has granted bioRxiv a license to display the preprint in perpetuity. It is made available under a CC-BY-NC-ND 4.0 International license.

Figure 6-figure supplement 1

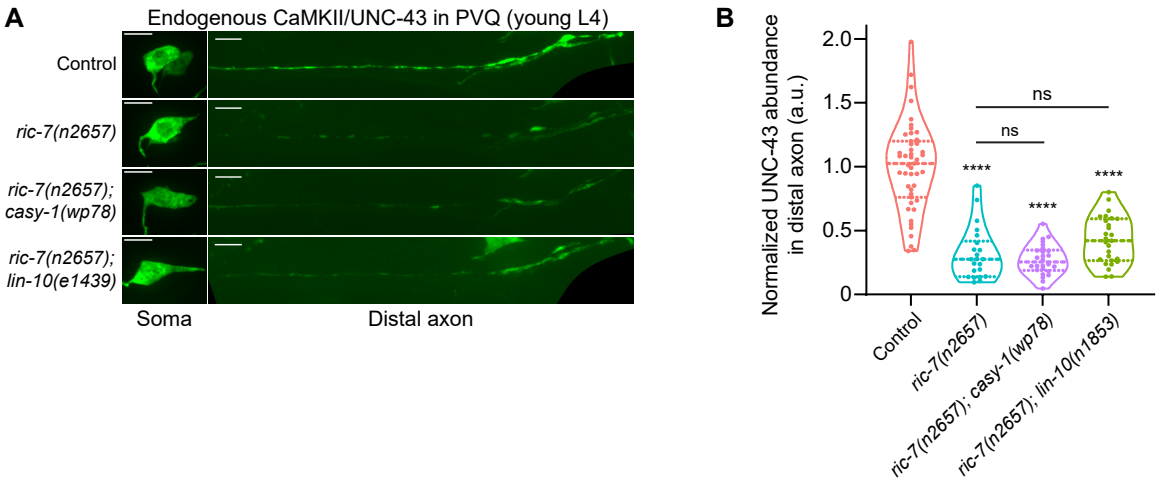

Figure 6-figure supplement 1. CaMKII/UNC-43 abundance in distal axons is not restored in *ric-7(n2657); casy-1(wp78)* and *ric-7(n2657); lin-10(e1439)* animals

(A) Images of NATF-tagged CaMKII/UNC-43 in PVQ cell bodies and distal axons in L4 stage animals. Genotypes: control, *ric-7(n2657)*, *ric-7(n2657); casy-1(wp78)*, and *ric-7(n2657); lin-10(e1439)*. Scale bar, 5 µm.

(B) Normalized NATF-tagged CaMKII/UNC-43 intensity (arbitrary units) in PVQ distal axons in control, *ric-7(n2657)*, *ric-7(n2657); casy-1(wp78)*, and *ric-7(n2657); lin-10(e1439)* animals at L4. Violin plots with median and quantiles are shown. **** indicates $p<0.0001$, ns = not significant, compared to control except where indicated, one-way ANOVA, Kruskal-Wallis test, followed by Dunn's multiple comparisons.

bioRxiv preprint doi: https://doi.org/10.1101/2021.09.12.459970; this version posted September 12, 2021. The copyright holder for this preprint (which was not certified by peer review) is the author/funder, who has granted bioRxiv a license to display the preprint in perpetuity. It is made available under a CC-BY-NC-ND 4.0 International license.

Figure 6-figure supplement 2

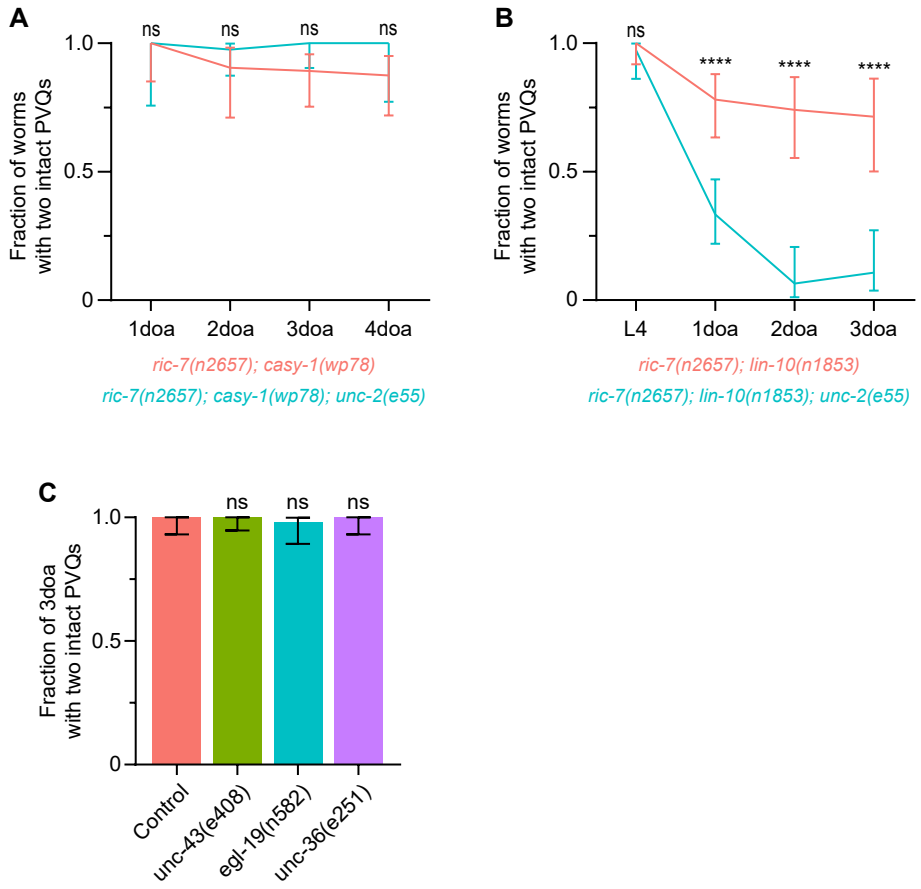

Figure 6-figure supplement 2. VGCC subunit *unc-2* does not mediate axon protection, and loss of CaMKII/*unc-43*, VGCC subunit *egl-19* or VGCC subunit *unc-36* does not result in axon degeneration

(A-B) Effect of the lof mutation, *unc-2(e55)*, on the protection against degeneration in *ric-7(n2657); casy-1(wp78)* (N = 13-41) and *ric-7(n2657); lin-10(n1853)* (N = 21-51) animals. Graphs show proportion and 95% CI. **** indicates p<0.0001, ns = not significant, Fisher's exact test.

(C) Quantification of axon degeneration in control (N = 52), *unc-43(e408)* (N = 69), *egl-19(n582)* (N = 49), *unc-36(e251)* (N = 52) 3doa. Bars show proportion and 95% CI. ns = not significant, compared to control, Fisher's exact test.